International Journal of Heat and Mass Transfer 222 (2024) 125055

Contents lists available at ScienceDirect

International Journal of Heat and Mass Transfer

journal homepage: www.elsevier.com/locate/ijhmt

Analytical modeling of phase change in a composite wall comprising two distinct phase change materials in series

Emad Hasrati [1], Girish Krishnan [1], Ankur Jain [*]

Mechanical and Aerospace Engineering Department, University of Texas at Arlington, Arlington, TX, United States of America

ARTICLE INFO

Keywords:
Phase change heat transfer
Multilayer wall
Moving boundary problems
Analytical Modeling
Melting and Solidification

ABSTRACT

Most of the past literature on solid-liquid phase change heat transfer modeling focuses on a single phase change material (PCM), whereas, a sandwich of two or more PCMs arranged in series may be of interest in several applications. The modeling of heat transfer and phase change in such a system is complicated by the presence of multiple phase change fronts propagating at the same time. This work presents a theoretical analysis of the problem of melting of a two-PCM stack being heated from one end. Depending on whether the lower-melting PCM is located next to or away from the heat source, two distinct cases are considered. The propagation of the phase change fronts in each case is divided into several stages, each of which is characterized by a distinct phase change and/or sensible heating processes. The transient temperature field in each stage is determined in the form of infinite series solutions, and the propagation of phase change front over time is then determined using energy conservation at the phase change interface. In this manner, explicit expressions are derived for the time taken for each layer to completely melt. Results are shown to be in good agreement with finite-element simulations, and with the exact Stefan solution under special conditions. Key non-dimensional parameters that influence the nature of the two-PCM phase change process are identified, and their impact on phase change performance is analyzed. Quantitative predictions are presented for the conditions under which both PCMs finish melting at the same time, which is a favorable outcome for efficient energy storage.

1. Introduction

Phase change heat transfer during melting and solidification [1,2] plays a key role in a number of engineering systems and processes, including thermal management [3], energy storage [4] and manufacturing [5]. Important performance parameters in such processes include total time taken for melting/freezing, total energy removed/stored and the efficiency of energy storage [6,7]. Moving boundary problems involving the phase change front often appear in the analysis of such applications and play a key role in determining these performance parameters.

Accurate theoretical models are critical for developing a fundamental understanding of phase change phenomena, and thus for designing and optimizing practical energy storage systems. Several complications, including moving boundaries, convective flow in the melted liquid, phase change over a temperature range and temperature-dependent properties result in an inherently non-linear problem [1,2]. Exact solutions are available only for very specific, relatively simple problems [1,8]. A number of approximate analysis methods have been developed for phase change problems, including quasi-steady method [2], eigenfunction-based techniques [9–11], integral-based techniques [12] and perturbation methods [13]. Most of these methods assume a sufficiently slow rate of growth of the melting front, i.e., a small value of the Stefan number. A number of numerical simulation techniques have also been developed for solving phase change heat transfer problems [2,14].

While most of the literature in phase change heat transfer considers the melting or freezing of a single material, the use of more than one phase change materials (PCMs) has also been considered to a limited extent. Fig. 1(a) shows an illustration of two PCM slabs arranged in series with an external heat source. Second law and exergy analysis [15–17] has shown that series arrangement of multiple PCMs with different melting temperatures in an energy storage system may result in lower exergy loss than a single PCM. The optimum melting temperatures of the PCMs based on thermodynamics considerations have been determined [15,18]. Motivated by such thermodynamic predictions, the use of two or more PCMs in series in an energy storage system has been

* Corresponding author at: 500 W First St, Rm 211, Arlington, TX 76019, USA.
E-mail address: jaina@uta.edu (A. Jain).
[1] Equal contributors.

https://doi.org/10.1016/j.ijheatmasstransfer.2023.125055
Received 18 April 2023; Received in revised form 8 September 2023; Accepted 6 December 2023
Available online 15 January 2024

Nomenclature

Bi	Biot number
C_p	heat capacity ($Jkg^{-1}K^{-1}$)
k	thermal conductivity ($Wm^{-1}K^{-1}$)
$\bar{k}_2$	ratio of thermal conductivities
L	layer thickness (m)
$\mathscr{L}$	latent heat of phase change (Jkg^{-1})
Ste	Stefan number
t	time (s)
T	temperature (K)
x	spatial coordinate (m)
α	thermal diffusivity (m^2s^{-1})
$\bar{\alpha}_2$	ratio of thermal diffusivities
γ	non-dimensional interface location
ϕ	non-dimensional melting temperature of higher-melting layer
τ	non-dimensional time
θ	non-dimensional temperature
ξ	non-dimensional spatial coordinate

Subscripts

A, B, C	stages
f	phase change temperature
w	wall
LS	phase change front location
$1, 2$	layer number

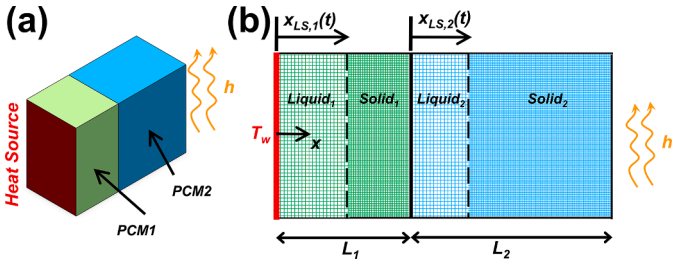

Fig. 1. (a) Schematic of the problem considered here, showing a stack of two PCMs subjected to heating from one end that results in phase change propagation in both layers. (b) Detailed geometry of the problem showing liquid and solid phases, as well as the phase change front locations in both layers at a specific time.

investigated through experimental measurements relevant to solar power plants [19] and thermal control of power electronics [20]. Measurements are available for both cylindrical [21–23] and slab-shaped [20,24] PCM geometries. Comparison between single-PCM and multi-PCM cases for practical scenarios involving a bed of encapsulated spherical capsules has been presented [25]. A multi-PCM energy storage problem involves a large number of parameters, several of which are difficult to vary independently in an experiment. For example, while experiments have been carried out to specifically investigate the effect of melting temperatures of three PCMs in a heat storage module [23], it is difficult, in general, to identify which non-dimensional parameters may be most influential in determining the performance characteristics of a multi-PCM energy storage system.

Despite the importance of theoretical modeling of the phase change processes in a multi-PCM energy storage system, there is, in general, a lack of literature in this direction. Phase change in a multi-PCM body is not a straightforward problem due to the presence of multiple complications and non-linearities. For example, the simultaneous presence of two melting fronts makes the problem considerably complicated. Further, depending on the relative rates of melting, thermal conduction will occur in melted or unmelted regions in parallel with phase change propagation. The phase change process may not be complete in all PCMs at the same time. Therefore, shielding effects caused by the melted material protecting unmelted material from the hot source (and vice versa during the freezing process) must be correctly accounted for.

Owing to the analytical complications outlined above, most of the literature on the analysis of multi-PCM energy systems is limited to numerical computation using finite-element [26] and finite-difference [27] techniques, and commercially available software [28,29]. Theoretical and numerical analysis of a special case containing an infinite number of PCMs has been presented [30]. The performance of series and parallel arrangements of multiple PCMs has been evaluated numerically [31]. The impact of convection in heat exchange with the external heat source has been evaluated numerically [32].

Despite such literature, an analytical solution for the temperature distribution and phase change front propagation in a multi-PCM problem may be a lot more valuable than numerical simulations in helping understand the fundamental nature of such a system. This may help, for example, identify key non-dimensional parameters and their impact on the phase change process, which may help optimize the performance of realistic systems. Key questions that an analytical model may help address include determining the layer that will finish melting first, the total time taken for melting and an optimal design of the multi-PCM stack to achieve desired system-level performance goals such as simultaneous completion of melting. While exact analytical solutions for phase change problems are available only in limited cases, even an approximate analytical solution, valid under specific conditions such as small Stefan number may be of much interest for design and optimization.

This work presents theoretical analysis of phase change in two slabs of different PCMs arranged in series and heated up by a constant temperature source at one end. Depending on the relative melting temperatures and placement of the two PCMs, two separate cases are considered. In each case, the melting process is systematically split into multiple stages, depending on which PCM has melted and which is still melting. Expressions for temperature distributions and rates of phase change propagation in both PCMs are derived using the method of eigenfunction expansion coupled with energy conservation at each phase change front. These theoretical results are used to understand the impact of thermophysical properties, relative thicknesses and placement of the PCMs on total melting time, as well as to determine the conditions in which both melt by the same time.

2. Problem definition

Consider the problem of phase change in a composite wall comprising two PCMs with distinct thermophysical properties, including melting temperature. The geometry of the problem is summarized in Fig. 1. The thicknesses of the two layers are L_1 and L_2, respectively. The phase change temperature, thermal conductivity, thermal diffusivity, heat capacity and latent heat are denoted by T_f, α, k, C_p and $\mathscr{L}$, with a subscript to denote the specific material 1 or 2. Phase change in this geometry is driven by the hot wall maintained at a fixed temperature T_w and in direct contact with layer 1 starting at $t = 0$. The other end of the geometry is subjected to convective cooling characterized by a convective heat transfer coefficient h, which, when set to zero or a very large number results in the special cases of adiabatic or isothermal boundary, respectively. This problem is posed here as a melting problem, i.e., $T_w > T_{f,1}$ and $T_w > T_{f,2}$, although a similar technique can be

used to analyze the opposite problem of freezing. One-dimensional heat diffusion and phase change propagation is assumed. Convective flow effects in the newly melted materials are neglected. This is a reasonable assumption for several applications in which the Rayleigh number is sufficiently small to neglect natural convection. Further, all thermophysical properties are assumed to be constant, uniform and independent of temperature. This is also a reasonable assumption in cases where the temperature rise is small.

This problem is characterized by two distinct phase change fronts that propagate towards the right. Due to the distinct melting temperatures and other thermophysical properties of the two materials, phase change in the two layers may propagate at different rates, and either simultaneously or in series. The phase change process will continue until both materials are completely melted. In general, the interest is in determining the temperature distributions $T_1(x,t)$ and $T_2(x,t)$, as well as the locations of the two phase change fronts $x_{LS,1}(t)$ and $x_{LS,2}(t)$, as shown in Fig. 1(b). Note that, with reference to Fig. 1(b), $x_{LS,1}(t)$ and $x_{LS,2}(t)$ are measured from the left ends of layers 1 and 2, respectively. In the coordinate system shown, $x_{LS,1}(t)$ is measured from $x = 0$ and $x_{LS,2}(t)$ from $x = L_1$. The total time taken for melting is also a global performance parameter of interest. Determining a design that results in simultaneous completion of melting in both layers is also of interest.

This problem is considerably complicated by the presence of two distinct but inter-dependent phase change fronts and shielding of the phase change front by previously melted material. A robust theoretical understanding and modeling of this problem must account for simultaneous diffusion and phase change within both materials. While exact solutions may exist for simplified problems such as one-dimensional phase change propagation in a single PCM [1], in the present case of two PCMs, an approximate analytical solution may need to be derived.

In order to analyze this two-PCM problem, two distinct cases are considered separately. In the first case, the melting temperature of the first layer next to the hot wall is lower than that of the second layer, i.e., $T_{f,1} < T_{f,2}$, and in the second case, $T_{f,1} > T_{f,2}$. Analyses of these cases are presented in two sub-sections below.

3. Solution of Case I: $T_{f,1} < T_{f,2}$

It is assumed that both materials are initially at a uniform temperature corresponding to the lower of the two melting temperatures, i.e., $T_{f,1}$. Since layer 1 melts at a temperature lower than layer 2 and is next to the hot source, therefore, layer 1 will begin to melt immediately. The melting front in layer 1 will then proceed rightwards until the entire layer 1 has melted. Since all regions beyond the melting front of the first layer must be at $T_{f,1}$, which is lower than $T_{f,2}$, therefore, no melting will occur in layer 2 until all of layer 1 has melted. Afterwards, sensible heating of the two layers will occur until the interface temperature reaches the melting temperature of the second layer, $T_{f,2}$. At this point, the second layer will begin to melt, and heat conducted through the first layer will continue to propagate the melting front of the second layer rightwards until all of layer 2 has melted.

It is helpful to split the entire process described above into three separate stages, each of which is characterized by distinct physical processes governed by a distinct set of equations. During Stage A, only layer 1 melts, whereas layer 2 temperature does not rise since the material behind the melting front must remain at the initial temperature. Stage A is complete when layer 1 is fully melted. This is followed by Stage B, during which, heat from the hot wall continues to conduct into the two layers, resulting in temperature rise in both layers but no further melting. Stage B is complete when the temperature at the interface reaches $T_{f,2}$. At this time, layer 2 is ready to melt. In the subsequent Stage C, layer 2 melts due to heat conducted into layer 2 from layer 1. Each of these Stages is solved in sequence. Temperature field at the end of each Stage provides the initial condition for the next Stage.

Before a mathematical description of each of these Stages is presented, it is helpful to non-dimensionalize the problem using the following scheme: $\xi = \frac{x}{L_1+L_2}$, $\tau = \frac{\alpha_1 t}{(L_1+L_2)^2}$, $\theta_i = \frac{T_i - T_{f,1}}{T_w - T_{f,1}}$, $Ste_i = \frac{C_{p,i}(T_w - T_{f,1})}{\mathscr{L}_i}$, $\xi_{LS,i} = \frac{x_{LS,i}}{L_1+L_2}$, $\phi_2 = \frac{T_{f,2} - T_{f,1}}{T_w - T_{f,1}}$, $\gamma = \frac{L_1}{L_1+L_2}$, $\bar{\alpha}_2 = \frac{\alpha_2}{\alpha_1}$, $\bar{k}_2 = \frac{k_2}{k_1}$; $Bi = \frac{h(L_1+L_2)}{k_1}$. Note that $i = 1,2$. The temperature difference $(T_w - T_{f,1})$ based on the lower of the two melting temperatures is used for non-dimensionalization. Based on this, the following sub-sections mathematically describe the temperature fields and melting front locations during each of the three Stages.

3.1. Stage A: melting of layer 1

Since $T_{f,1} < T_{f,2}$, therefore, only layer 1 melts during Stage A, because until all of layer 1 has melted, layer 2 temperature can not begin to rise above the initial temperature. Therefore, during Stage A, $\theta_2(\xi,\tau) = 0$ throughout and $\xi_{LS,2}(\tau) = 0$. Note that $\xi_{LS,2}$ is measured relative to the interface located at $\xi = \gamma$. On the other hand, temperature field in the melted region of layer 1 $(0 < \xi < \xi_{LS,1}(\tau))$ satisfies the following conservation equation [2]

$$\frac{\partial^2 \theta_1}{\partial \xi^2} = \frac{\partial \theta_1}{\partial \tau} \tag{1}$$

along with the following boundary conditions:

$$\theta_1 = 1, \quad (\xi = 0) \tag{2}$$

$$\theta_1 = 0, \quad \left(\xi = \xi_{LS,1}(\tau)\right) \tag{3}$$

$$\frac{d\xi_{LS,1}}{d\tau} = -Ste_1 \left(\frac{\partial \theta_1}{\partial \xi}\right)_{\xi = \xi_{LS,1}} \tag{4}$$

The melting problem represented by Eqs. (1)-(4) is a straightforward one-dimensional Stefan problem with constant wall temperature, for which, the well-known analytical solution is given by [1]

$$\theta_1(\xi,\tau) = 1 - \frac{\mathrm{erf}\left(\frac{\xi}{2\sqrt{\tau}}\right)}{\mathrm{erf}\left(\frac{\xi_{LS,1}}{2\sqrt{\tau}}\right)} \tag{5}$$

in the region $0 < \xi < \xi_{LS,1}$. The melting front location is given by [1]

$$\xi_{LS,1}(\tau) = 2\lambda\sqrt{\tau} \tag{6}$$

where λ satisfies the equation $x \cdot \mathrm{erf}(x) \cdot \exp(x^2) = \frac{Ste_1}{\sqrt{\pi}}$.

In the remainder of layer 1 beyond the melting front as well as all of layer 2, the temperature remains unchanged during Stage A, i.e., $\theta_1(\xi,\tau) = 0$ for $\xi_{LS,1}(\tau) < \xi < \gamma$ and $\theta_2(\xi,\tau) = 0$ for $\gamma < \xi < 1$. This completes the mathematical description of the temperature fields and melting front locations during Stage A. This Stage ends at $\tau = \tau_A^*$ when the melting front in the first layer reaches the interface between the two layers. Mathematically, this may be written as $\xi_{LS,1}(\tau_A^*) = \gamma$, or, from Eq. (6), $\tau_A^* = \gamma^2/4\lambda^2$. Using Eq. (5), the temperature distribution in layer 1 at $\tau = \tau_A^*$, $\theta_{1,A}^*(\xi) = 1 - \frac{\mathrm{erf}(\xi\lambda/\gamma)}{\mathrm{erf}(\lambda)}$ provides the initial condition for Stage B, which is described in detail next.

3.2. Stage B: sensible heating of layers 1 and 2

In Stage B, sensible heating and temperature rise occurs in both layers – layer 1, which is already completely melted and layer 2, which is still solid and below its melting temperature. The completion of Stage B corresponds to the interface between layers reaching the melting temperature of layer 2, ϕ_2, at which point, layer 2 is ready to melt.

Since no phase change occurs during Stage B, therefore, both melting

fronts remain stationary, i.e., $\xi_{LS,1}(\tau) = \gamma$, $\xi_{LS,2}(\tau) = 0$ throughout. However, the temperature field does evolve due to diffusion of heat into the layers. The temperature field in layer 1, θ_1 satisfies the conservation equation given by Eq. (1) for $0 < \xi < \gamma$, whereas, in the region $\gamma < \xi < 1$, the temperature field in layer 2, θ_2 satisfies a similar equation given by [2]

$$\frac{\partial^2\theta_2}{\partial\xi^2} = \frac{1}{\bar{\alpha}_2}\frac{\partial\theta_2}{\partial\tau} \tag{7}$$

The two temperature fields also satisfy boundary and interface conditions given by Eq. (2) as well as

$$\theta_1 = \theta_2, \qquad (\xi = \gamma) \tag{8}$$

$$\frac{\partial\theta_1}{\partial\xi} = \bar{k}_2\frac{\partial\theta_2}{\partial\xi}, \qquad (\xi = \gamma) \tag{9}$$

$$-\bar{k}_2\frac{\partial\theta_2}{\partial\xi} = Bi\cdot\theta_2, (\xi = 1) \tag{10}$$

The initial condition for this pure-diffusion two-layer problem is given by the final temperature at the end of Stage A for layer 1 and zero temperature for layer 2, i.e.,

$$\theta_1 = \theta^*_{1,A}(\xi);\ \theta_2 = 0, \quad (\tau = \tau^*_A) \tag{11}$$

This problem can be solved using separation of variables method and the use of quasi-orthogonality of multilayer eigenfunctions [14,33]. In brief, the temperature fields are first split into two components in order to account for the non-homogeneity in the boundary condition. Then, by requiring the solution to satisfy the boundary and interface conditions given by Eqs. (2) and (8)-(10), it can be shown that the solution is given by

$$\theta_1(\xi,\tau) = 1 + \frac{\bar{k}_2}{\gamma(1-\bar{k}_2) - \frac{\bar{k}_2+Bi}{Bi}}\xi + \sum_{n=1}^{\infty} c_n \sin(\omega_n\xi)\exp\left(-\omega_n^2(\tau-\tau^*_A)\right) \tag{12}$$

$$\theta_2(\xi,\tau) = \frac{-(\bar{k}_2+Bi)}{Bi\left(\gamma(1-\bar{k}_2) - \frac{\bar{k}_2+Bi}{Bi}\right)}\left(1 - \frac{Bi}{\bar{k}_2+Bi}\xi\right) + \sum_{n=1}^{\infty} c_n\left[\left(\sin(\omega_n\gamma)\cos\left(\frac{\omega_n\gamma}{\sqrt{\bar{\alpha}_2}}\right) - \frac{\sqrt{\bar{\alpha}_2}}{\bar{k}_2}\cos(\omega_n\gamma)\sin\left(\frac{\omega_n\gamma}{\sqrt{\bar{\alpha}_2}}\right)\right)\right.$$
$$\left.\cos\left(\frac{\omega_n}{\sqrt{\bar{\alpha}_2}}\xi\right) + \left(\sin(\omega_n\gamma)\sin\left(\frac{\omega_n\gamma}{\sqrt{\bar{\alpha}_2}}\right) + \frac{\sqrt{\bar{\alpha}_2}}{\bar{k}_2}\cos(\omega_n\gamma)\cos\left(\frac{\omega_n\gamma}{\sqrt{\bar{\alpha}_2}}\right)\right)\sin\left(\frac{\omega_n}{\sqrt{\bar{\alpha}_2}}\xi\right)\right]\exp\left(-\omega_n^2(\tau-\tau^*_A)\right) \tag{13}$$

where the eigenvalues ω_n are given by roots of the following eigenfunction

$$\frac{\sin(x\gamma)\cos\left(\frac{x\gamma}{\sqrt{\bar{\alpha}_2}}\right) - \frac{\sqrt{\bar{\alpha}_2}}{\bar{k}_2}\cos(x\gamma)\sin\left(\frac{x\gamma}{\sqrt{\bar{\alpha}_2}}\right)}{Bi\sin\left(\frac{x}{\sqrt{\bar{\alpha}_2}}\right) + \frac{\bar{k}_2}{\sqrt{\bar{\alpha}_2}}x\cos\left(\frac{x}{\sqrt{\bar{\alpha}_2}}\right)} + \frac{\sin(x\gamma)\sin\left(\frac{x\gamma}{\sqrt{\bar{\alpha}_2}}\right) + \frac{\sqrt{\bar{\alpha}_2}}{\bar{k}_2}\cos(x\gamma)\cos\left(\frac{x\gamma}{\sqrt{\bar{\alpha}_2}}\right)}{Bi\cos\left(\frac{x}{\sqrt{\bar{\alpha}_2}}\right) + \frac{\bar{k}_2}{\sqrt{\bar{\alpha}_2}}x\cos\left(\frac{x}{\sqrt{\bar{\alpha}_2}}\right)} = 0 \tag{14}$$

and the coefficients c_n are given by

$$c_n = \frac{1}{N_n}\left[\int_0^{\gamma}\left(\theta^*_{1A}(\xi) - \left(1 + \frac{\bar{k}_2}{\gamma(1-\bar{k}_2) - \frac{\bar{k}_2+Bi}{Bi}}\xi\right)\right)\sin(\omega_n\xi)d\xi\right.$$
$$- \frac{\bar{k}_2}{\bar{\alpha}_2}\int_{\gamma}^{1}\left(\frac{-(\bar{k}_2+Bi)}{Bi\left(\gamma(1-\bar{k}_2) - \frac{\bar{k}_2+Bi}{Bi}\right)}\left(1 - \frac{Bi}{\bar{k}_2+Bi}\xi\right)\right)\left[\left(\sin(\omega_n\gamma)\cos\left(\frac{\omega_n\gamma}{\sqrt{\bar{\alpha}_2}}\right)\right.\right.$$
$$\left.\left. - \frac{\sqrt{\bar{\alpha}_2}}{\bar{k}_2}\cos(\omega_n\gamma)\sin\left(\frac{\omega_n\gamma}{\sqrt{\bar{\alpha}_2}}\right)\right)\cos\left(\frac{\omega_n}{\sqrt{\bar{\alpha}_2}}\xi\right) + \left(\sin(\omega_n\gamma)\sin\left(\frac{\omega_n\gamma}{\sqrt{\bar{\alpha}_2}}\right)\right.\right.$$
$$\left.\left.\left. + \frac{\sqrt{\bar{\alpha}_2}}{\bar{k}_2}\cos(\omega_n\gamma)\cos\left(\frac{\omega_n\gamma}{\sqrt{\bar{\alpha}_2}}\right)\right)\sin\left(\frac{\omega_n}{\sqrt{\bar{\alpha}_2}}\xi\right)\right]d\xi\right] \tag{15}$$

and the norms N_n are given by

$$N_n = \int_0^{\gamma}\sin^2(\omega_n\xi)d\xi + \frac{\bar{k}_2}{\bar{\alpha}_2}\int_{\gamma}^{1}\left[\left(\sin(\omega_n\gamma)\cos\left(\frac{\omega_n\gamma}{\sqrt{\bar{\alpha}_2}}\right) - \frac{\sqrt{\bar{\alpha}_2}}{\bar{k}_2}\cos(\omega_n\gamma)\sin\left(\frac{\omega_n\gamma}{\sqrt{\bar{\alpha}_2}}\right)\right)\cos\left(\frac{\omega_n}{\sqrt{\bar{\alpha}_2}}\xi\right) + \left(\sin(\omega_n\gamma)\sin\left(\frac{\omega_n\gamma}{\sqrt{\bar{\alpha}_2}}\right) + \frac{\sqrt{\bar{\alpha}_2}}{\bar{k}_2}\cos(\omega_n\gamma)\cos\left(\frac{\omega_n\gamma}{\sqrt{\bar{\alpha}_2}}\right)\right)\sin\left(\frac{\omega_n}{\sqrt{\bar{\alpha}_2}}\xi\right)\right]^2 d\xi \tag{16}$$

Since Stage B involves only diffusion while layer 2 is below its melting temperature and layer 1 has already fully melted, therefore, the melting fronts remain stationary during this Stage. Stage B finishes at $\tau = \tau^*_B$ when the temperature at the interface reaches the melting temperature of layer 2, i.e., $\theta_1(\gamma, \tau^*_B) = \phi_2$. By combining this requirement with Eq. (12), it can be shown that τ^*_B is given by the root of the following equation:

$$\sum_{n=1}^{\infty} c_n \sin(\omega_n\gamma)\exp\left(-\omega_n^2(\tau-\tau^*_A)\right) = \phi_2 - 1 - \frac{\bar{k}_2}{\gamma(1-\bar{k}_2) - \frac{\bar{k}_2+Bi}{Bi}}\gamma \tag{17}$$

The final temperature fields in the two layers at $\tau = \tau_B^*$ are given by

$$\theta_{1,B}^*(\xi) = 1 + \frac{\bar{k}_2}{\gamma(1-\bar{k}_2) - \frac{\bar{k}_2+Bi}{Bi}}\xi + \sum_{n=1}^{\infty} c_n \sin(\omega_n \xi)\exp\left(-\omega_n^2(\tau_B^* - \tau_A^*)\right) \quad (18)$$

$$\begin{aligned}\theta_{2,B}^*(\xi) =& \frac{-(\bar{k}_2+Bi)}{Bi\left(\gamma(1-\bar{k}_2) - \frac{\bar{k}_2+Bi}{Bi}\right)}\left(1 - \frac{Bi}{\bar{k}_2+Bi}\xi\right) \\ &+ \sum_{n=1}^{\infty} c_n \left[\left(\sin(\omega_n\gamma)\cos\left(\frac{\omega_n\gamma}{\sqrt{\bar{\alpha}_2}}\right) - \frac{\sqrt{\bar{\alpha}_2}}{\bar{k}_2}\cos(\omega_n\gamma)\sin\left(\frac{\omega_n\gamma}{\sqrt{\bar{\alpha}_2}}\right)\right)\right. \\ &\cos\left(\frac{\omega_n}{\sqrt{\bar{\alpha}_2}}\xi\right) - \left(\sin(\omega_n\gamma)\sin\left(\frac{\omega_n\gamma}{\sqrt{\bar{\alpha}_2}}\right) + \frac{\sqrt{\bar{\alpha}_2}}{\bar{k}_2}\cos(\omega_n\gamma)\cos\left(\frac{\omega_n\gamma}{\sqrt{\bar{\alpha}_2}}\right)\right) \\ &\left.\sin\left(\frac{\omega_n}{\sqrt{\bar{\alpha}_2}}\xi\right)\right]\exp\left(-\omega_n^2(\tau_B^* - \tau_A^*)\right)\end{aligned} \quad (19)$$

3.3. Stage C: sensible heating of layer 1 and melting of layer 2

At the end of Stage B, the temperature at the interface between layers is ϕ_2 and layer 2 is now ready to undergo phase change. Further thermal conduction causes the initiation of phase change in layer 2. Therefore, Stage C is characterized by the melting of layer 2 caused by heat conducted into the layer through the already melted layer 1. Only sensible heating occurs in layer 1. Moreover, some heat transfer into the solid region of layer 2 beyond its melting front also occurs.

The problem of phase change of a material mediated by thermal conduction through other non-melting layers has been solved recently [10,11]. In the present case, at any time, one may consider the melted region of layer 2, ($\gamma < \xi < \gamma + \xi_{LS,2}(\tau)$) to be sandwiched between two non-melting regions – layer 1 ($0 < \xi < \gamma$) and the unmelted region of layer 2 ($\gamma + \xi_{LS,2}(\tau) < \xi < 1$). For convenience, the two regions of layer 2 are denoted as 2a and 2b, respectively.

Based on the recently developed technique for solving such problems [10,11], expressions for temperature distributions in the three layers are written in order to satisfy the respective governing equations. Eigenvalues of the problem and various coefficients appearing in the series solution are determined by requiring the solution to satisfy various boundary and interface conditions, along with the use of principle of quasi-orthogonality of the eigenfunctions. In the present case during Stage C, the temperature distribution in layer 1 satisfies Eq. (1) in the range $0 < \xi < \gamma$, whereas temperature distribution in layers 2a and 2b satisfy Eq. (7) in the range $\gamma < \xi < \gamma + \xi_{LS,2}(\tau)$ and $\gamma + \xi_{LS,2}(\tau) < \xi < 1$, respectively. The initial condition for the temperature field comes from the temperature field at the end of the previous Stage.

The problem for layer 2b is uncoupled from the other two layers since the boundary conditions for this layer ($\theta_{2b} = \phi_2$ at $\xi = \gamma + \xi_{LS,2}$ and $-\bar{k}_2\frac{\partial\theta_{2b}}{\partial\xi} = Bi\cdot\theta_{2b}$ at $\xi = 1$) are completely independent of the other two layers. This problem can be solved directly using the method of separation of variables, resulting in the following solution for temperature field in layer 2b:

$$\begin{aligned}\theta_{2b}(\xi,\tau) =& \phi_2\left(1 + \frac{Bi}{\bar{k}_2 + Bi(1-\gamma-\xi_{LS,2})}(\gamma + \xi_{LS,2} - \xi)\right) \\ &+ \sum_{n=1}^{\infty}\widehat{c}_n\left[\cos\left(\frac{\widehat{\omega}_n}{\sqrt{\bar{\alpha}_2}}\xi\right) - \cot\left(\frac{\widehat{\omega}_n}{\sqrt{\bar{\alpha}_2}}(\gamma+\xi_{LS,2})\right)\sin\left(\frac{\widehat{\omega}_n}{\sqrt{\bar{\alpha}_2}}\xi\right)\right]\exp\left(\right. \\ &\left.-\widehat{\omega}_n^2(\tau - \tau_B^*)\right)\end{aligned} \quad (20)$$

where the eigenvalues $\widehat{\omega}_n$ are roots of

$$\frac{\frac{\bar{k}_2 x}{\sqrt{\bar{\alpha}_2}} - Bi\cot\left(\frac{x}{\sqrt{\bar{\alpha}_2}}\right)}{\cot\left(\frac{x}{\sqrt{\bar{\alpha}_2}}(\gamma+\xi_{LS,2})\right)} + \frac{\bar{k}_2 x}{\sqrt{\bar{\alpha}_2}}\cot\left(\frac{x}{\sqrt{\bar{\alpha}_2}}\right) + Bi = 0 \quad (21)$$

Since the initial temperature at $\tau = \tau_B^*$ for this problem is given by $\theta_{2,B}^*(\xi)$, therefore, using the principle of orthogonality, the coefficients $\widehat{c}_n$ may be written as

$$\begin{aligned}\widehat{c}_n =& \frac{1}{\widehat{N}_n}\int_{\gamma+\xi_{LS,2}}^{1}\left[\theta_{2,B}^*(\xi) - \phi_2\left(1 + \frac{Bi}{\bar{k}_2 + Bi(1-\gamma-\xi_{LS,2})}(\gamma + \xi_{LS,2} - \xi)\right)\right] \\ &\left[\cos\left(\frac{\widehat{\omega}_n}{\sqrt{\bar{\alpha}_2}}\xi\right) - \cot\left(\frac{\widehat{\omega}_n}{\sqrt{\bar{\alpha}_2}}(\gamma+\xi_{LS,2})\right)\sin\left(\frac{\widehat{\omega}_n}{\sqrt{\bar{\alpha}_2}}\xi\right)\right]d\xi\end{aligned} \quad (22)$$

and

$$\widehat{N}_n = \int_{\gamma+\xi_{LS,2}}^{1}\left[\cos\left(\frac{\widehat{\omega}_n}{\sqrt{\bar{\alpha}_2}}\xi\right) - \cot\left(\frac{\widehat{\omega}_n}{\sqrt{\bar{\alpha}_2}}(\gamma+\xi_{LS,2})\right)\sin\left(\frac{\widehat{\omega}_n}{\sqrt{\bar{\alpha}_2}}\xi\right)\right]^2 d\xi \quad (23)$$

In contrast with layer 2b, the problems in layers 1 and 2a are coupled with each other due to the interface conditions at $\xi = \gamma$. Three boundary and interface conditions for the problem are given by Eqs. (2), (8) and (9), respectively. Additionally, temperature at $\xi = \gamma + \xi_{LS,2}(\tau)$ must be equal to the melting temperature ϕ_2. A solution for the two temperature fields may be derived by first splitting into two parts to account for the non-homogeneity and then writing a series solution for the remainder. When inserted into the boundary and interface conditions, this results in a set of four homogeneous equations in the coefficients appearing in the series solution. The determinant of these equations is then required to be zero in order to ensure a non-trivial solution, which results in the eigenequation. Finally, the remaining coefficients are determined using the initial condition, given by the temperature distribution at the end of Stage B, and the principle of quasi-orthogonality. Complete details of this technique may be found in a recent paper that solved the problem of phase change propagation in a PCM due to heat diffusing through a non-melting layer [10]. The final solution is found to be

$$\theta_1(\xi,\tau) = 1 - \frac{\bar{k}_2(1-\phi_2)\xi}{\gamma\bar{k}_2 + \xi_{LS,2}} + \sum_{n=1}^{\infty} c_n \sin(\omega_n\xi)\exp\left(-\omega_n^2(\tau - \tau_B^*)\right) \quad (24)$$

Table 1
Summary of governing equations and results for temperature profiles and melting front locations in various Stages of the two Cases considered in this work.

Case I: $T_{f,1} < T_{f,2}$	**Governing equation**	**Temperature profile**	**Phase change front location**
Stage A: Melting of layer 1	(1)	(5)	(6)
Stage B: Sensible heating of both layers	(1), (7)	(12)-(16)	No melting occurs in this Stage
Stage C: Melting of layer 2	(1), (7)	(20)-(28)	(29)
Case II: $T_{f,1} > T_{f,2}$	**Governing equation**	**Temperature profile**	**Phase change front location**
Stage A: Melting of layers 1 and 2	(1), (7)	(30)-(36)	(37)-(38)
Stage B: Melting of layer 2 (if layer 1 has fully melted in Stage A)	(1), (7)	(43)-(47)	(48)
Stage B: Melting of layer 1 (if layer 2 has fully melted in Stage A)	(1), (7)	(49)-(55)	(56)

$$\theta_{2a}(\xi,\tau)=\frac{\gamma+\xi_{LS,2}-\phi_2\gamma(1-\bar{k}_2)-(1-\phi_2)\xi}{\gamma\bar{k}_2+\xi_{LS,2}}+\sum_{n=1}^{\infty}c_n\left(\sin(\omega_n\gamma)\cos\left(\frac{\omega_n(\gamma-\xi)}{\sqrt{\bar{\alpha}_2}}\right)-\frac{\sqrt{\bar{\alpha}_2}}{\bar{k}_2}\cos(\omega_n\gamma)\sin\left(\frac{\omega_n(\gamma-\xi)}{\sqrt{\bar{\alpha}_2}}\right)\right)\exp\left(-\omega_n^2(\tau-\tau_B^*)\right) \tag{25}$$

where the eigenvalues ω_n are roots of

$$\cot\left(\frac{x\xi_{LS,2}}{\sqrt{\bar{\alpha}_2}}\right)+\frac{\sqrt{\bar{\alpha}_2}}{\bar{k}_2}\cot(x\gamma)=0 \tag{26}$$

Further, similar to the layer 2b problem, the coefficients c_n are obtained using the initial condition at $\tau=\tau_B^*$ as follows:

$$c_n=\frac{1}{N_n}\left[\int_0^{\gamma}\left(\theta_{1,B}^*(\xi)-1+\frac{\bar{k}_2(1-\phi_2)\xi}{\gamma\bar{k}_2+\xi_{LS,2}}\right)\sin(\omega_n\xi)d\xi+\frac{\bar{k}_2}{\bar{\alpha}_2}\int_{\gamma}^{\gamma+\xi_{LS,2}}\left(\theta_{2,B}^*(\xi)-\frac{\gamma+\xi_{LS,2}-\phi_2\gamma(1-\bar{k}_2)-(1-\phi_2)\xi}{\gamma\bar{k}_2+\xi_{LS,2}}\right)\left(\sin(\omega_n\gamma)\cos\left(\frac{\omega_n(\gamma-\xi)}{\sqrt{\bar{\alpha}_2}}\right)-\frac{\sqrt{\bar{\alpha}_2}}{\bar{k}_2}\cos(\omega_n\gamma)\sin\left(\frac{\omega_n(\gamma-\xi)}{\sqrt{\bar{\alpha}_2}}\right)\right)d\xi\right] \tag{27}$$

where

$$N_n=\int_0^{\gamma}\sin^2(\omega_n\xi)d\xi+\frac{\bar{k}_2}{\bar{\alpha}_2}\int_{\gamma}^{\gamma+\xi_{LS,2}}\left(\sin(\omega_n\gamma)\cos\left(\frac{\omega_n(\gamma-\xi)}{\sqrt{\bar{\alpha}_2}}\right)-\frac{\sqrt{\bar{\alpha}_2}}{\bar{k}_2}\cos(\omega_n\gamma)\sin\left(\frac{\omega_n(\gamma-\xi)}{\sqrt{\bar{\alpha}_2}}\right)\right)^2d\xi \tag{28}$$

Once solved, the rate of growth of the melting front in layer 2 may be written as

$$\frac{d\xi_{LS,2}}{d\tau}=-\bar{\alpha}_2Ste_2\left[\left(\frac{\partial\theta_{2a}}{\partial\xi}\right)-\left(\frac{\partial\theta_{2b}}{\partial\xi}\right)\right]_{\xi=\gamma+\xi_{LS,2}}=-\bar{\alpha}_2Ste_2\left[\frac{\phi_2-1}{\gamma\bar{k}_2+\xi_{LS,2}}+\sum_{n=1}^{\infty}c_n\frac{\omega_n}{\sqrt{\bar{\alpha}_2}}\left[-\sin(\omega_n\gamma)\sin\left(\frac{\omega_n\xi_{LS,2}}{\sqrt{\bar{\alpha}_2}}\right)+\frac{\sqrt{\bar{\alpha}_2}}{\bar{k}_2}\cos(\omega_n\gamma)\cos\left(\frac{\omega_n\xi_{LS,2}}{\sqrt{\bar{\alpha}_2}}\right)\right]\right.$$
$$\left.\exp\left(-\omega_n^2(\tau-\tau_B^*)\right)+\phi_2\frac{Bi}{\bar{k}_2+Bi(1-\gamma-\xi_{LS,2})}+\sum_{n=1}^{\infty}\widehat{c}_n\frac{\widehat{\omega}_n}{\sqrt{\bar{\alpha}_2}}\left[\sin\left(\frac{\widehat{\omega}_n(\gamma+\xi_{LS,2})}{\sqrt{\bar{\alpha}_2}}\right)+\cot\left(\frac{\widehat{\omega}_n}{\sqrt{\bar{\alpha}_2}}(\gamma+\xi_{LS,2})\right)\cos\left(\frac{\widehat{\omega}_n(\gamma+\xi_{LS,2})}{\sqrt{\bar{\alpha}_2}}\right)\right]\exp\left(-\widehat{\omega}_n^2(\tau-\tau_B^*)\right)\right] \tag{29}$$

The initial condition for Eq. (28) is given by $\xi_{LS,2}(\tau_B^*)=0$. Eq. (29) provides an explicit expression for the rate of change of $\xi_{LS,2}$ at any time, from where, $\xi_{LS,2}$ can be computed as a function of time. This completes the solution of the melting problem during Stage C, which finishes at $\tau=\tau_C^*$ when the melting front in layer 2 reaches the right-side end of the geometry, i.e., $\xi_{LS,2}(\tau_C^*)=1-\gamma$.

Taken together, the temperature distributions and locations of the two melting fronts described above in each Stage completely describe the solution for Case I of the two-PCM problem, in which, the material of the first layer melts at a temperature lower than that of the second layer. The total melting time is given simply by τ_C^*. A summary of governing equations and equations that describe the temperature field and phase change front location during each Stage for this Case is presented in Table 1.

Case II, in which, the melting temperature of the material of the second layer is lower is considered in the next sub-section.

4. Solution of Case II: $T_{f,1} > T_{f,2}$

In this case, the first layer melts at a higher temperature than the second layer. It is helpful to non-dimensionalize this problem slightly differently by using $T_{f,2}$ instead of $T_{f,1}$ as follows: $\theta_i=\frac{T_i-T_{f,2}}{T_w-T_{f,2}}$, $Ste_i=\frac{C_{p,i}(T_w-T_{f,2})}{\mathscr{L}_i}$, $\phi_1=\frac{T_{f,1}-T_{f,2}}{T_w-T_{f,2}}$. Note that $i=1,2$. Other non-dimensionalization definitions are the same as Case I. It is assumed that both layers are initially at the lower of the two melting temperatures, i.e., $\theta_i(\xi,0)=0$ $(i=1,\ 2)$.

Unlike Case I where the two layers melt in series, in this Case, thermal transport from the hot wall raises the temperature in some regions in both layers to above their respective melting temperature immediately after $\tau=0$. Therefore, the melting processes in the two layers proceed in parallel with each other. This makes the mathematical analysis for Case II somewhat more complicated compared to Case I.

Heat transfer and phase change in Case II is divided into two distinct Stages – in Stage A, both layers melt simultaneously and by the end of Stage A, either layer 1 or layer 2 has melted completely. The specific nature of heat transfer and phase change in Stage B is determined by which layer has melted completely in Stage A. Therefore, two distinct scenarios in Stage B must be considered separately.

4.1. Stage A: melting of layers 1 and 2

As soon as the two-layer body is exposed to high temperature on the left wall, thermal conduction from the left wall results in the initiation of melting in both layers 1 and 2. The two melting fronts simultaneously propagate rightwards in both layers until one of the layers is completely melted. Stage A of this Case considers this time duration, starting from $\tau=0$ when the heating process begins. During this time, $\xi_{LS,1}(\tau)$ and $\xi_{LS,2}(\tau)$ represent the locations of the two melting fronts, respectively, measured from the left side and from the interface, respectively. Accordingly, the entire region may be split into three sub-regions with non-zero temperature fields – region 1a comprising the melted region of layer 1 ($0<\xi<\xi_{LS,1}(\tau)$), region 1b comprising the solid region of layer 1 ($\xi_{LS,1}(\tau)<\xi<\gamma$), and region 2 comprising the melted region of layer 2 ($\gamma<\xi<\gamma+\xi_{LS,2}(\tau)$). Note that layer 2 beyond the melting front, i.e., $\xi>\gamma+\xi_{LS,2}(\tau)$ remains at zero temperature and, therefore, does not participate in heat transfer.

In order to determine the temperature fields in these regions, as well as the locations of the melting fronts, the governing energy equations and associated boundary/interface conditions must be written and solved. Firstly, the temperature field in the region 1a, $\theta_{1a}(\xi,\tau)$, satisfies Eq. (1) in the region $0<\xi<\xi_{LS,1}(\tau)$, as well as the boundary conditions given by $\theta_{1a}=1$ at $\xi=0$ and $\theta_{1a}=\phi_1$ at $\xi=\xi_{LS,1}$. Finally, this region is initially at zero temperature. This problem can be easily solved by first splitting into two parts to account for the non-homogeneities in the

boundary conditions, followed by use of the separation of variables method. This results in the following temperature distribution in region 1(a)

$$\theta_{1a}(\xi,\tau)=1-(1-\phi_1)\frac{\xi}{\xi_{LS,1}}+\sum_{n=1}^{\infty}\widehat{c}_n\sin(\widehat{\omega}_n\xi)\exp\left(-\widehat{\omega}_n^2\tau\right) \tag{30}$$

where $\widehat{\omega}_n=\frac{n\pi}{\xi_{LS,1}}$ and coefficients $\widehat{c}_n$ are obtained using orthogonality as follows:

$$\widehat{c}_n=\frac{2}{\xi_{LS,1}}\int_0^{\xi_{LS,1}}-\left[1-(1-\phi_1)\frac{\xi}{\xi_{LS,1}}\right]\sin(\widehat{\omega}_n\xi)d\xi \tag{31}$$

The temperature fields in regions 1b and 2a satisfy the conservation equations given by Eqs. (1) and (7) in regions $\xi_{LS,1}(\tau)<\xi<\gamma$ and $\gamma<\xi<\gamma+\xi_{LS,2}(\tau)$, respectively. Unlike the temperature field in region 1a, these temperature fields are coupled with each other through the interface conditions. The boundary and interface conditions for these regions are given by $\theta_{1b}=\phi_1$ at $\xi=\xi_{LS,1}$, $\theta_{2a}=0$ at $\xi=\gamma+\xi_{LS,2}$, $\theta_{1b}=\theta_{2a}$ at $\xi=\gamma$ and $\frac{\partial\theta_{1b}}{\partial\xi}=\bar{k}_2\frac{\partial\theta_{2a}}{\partial\xi}$ at $\xi=\gamma$. Both temperature fields are initially zero. In order to derive a solution for this two-layer diffusion problem, a substitution may first be carried out to account for the non-homogeneity in the boundary condition at $\xi=\xi_{LS,1}$. This may be followed by writing series solutions for each temperature field using a single set of eigenvalues, then using the homogenized boundary and interface conditions to derive an eigenequation and determine the coefficients in the series solution. The last remaining coefficient may then be derived using the initial condition and the principle of quasi-orthogonality of eigenfunctions. The details of these mathematical procedures may be found in well-known textbooks [14,34]. Following these steps, the final solutions for the temperature distributions may be derived as follows

$$\theta_{1b}(\xi,\tau)=\phi_1\frac{\bar{k}_2\xi-\bar{k}_2\gamma-\xi_{LS,2}}{\bar{k}_2\xi_{LS,1}-\bar{k}_2\gamma-\xi_{LS,2}}+\sum_{n=1}^{\infty}c_n\sin\left(\omega_n\left(\xi_{LS,1}-\xi\right)\right)\exp\left(-\omega_n^2\tau\right) \tag{32}$$

$$\begin{aligned}\theta_{2a}(\xi,\tau)=&\phi_1\frac{\xi-\gamma-\xi_{LS,2}}{\bar{k}_2\xi_{LS,1}-\bar{k}_2\gamma-\xi_{LS,2}}+\sum_{n=1}^{\infty}c_n\Bigg(\sin\left(\omega_n\left(\xi_{LS,1}-\gamma\right)\right)\\&\cos\left(\frac{\omega_n(\xi-\gamma)}{\sqrt{\bar{\alpha}_2}}\right)-\frac{\sqrt{\bar{\alpha}_2}}{\bar{k}_2}\cos\left(\omega_n\left(\xi_{LS,1}-\gamma\right)\right)\\&\sin\left(\frac{\omega_n(\xi-\gamma)}{\sqrt{\bar{\alpha}_2}}\right)\Bigg)\exp\left(-\omega_n^2\tau\right)\end{aligned} \tag{33}$$

where the eigenvalues ω_n are given by roots of the following eigenequation

$$\cot\left(\frac{x\xi_{LS,2}}{\sqrt{\bar{\alpha}_2}}\right)-\frac{\sqrt{\bar{\alpha}_2}}{\bar{k}_2}\cot\left(x\left(\xi_{LS,1}-\gamma\right)\right)=0 \tag{34}$$

and the coefficients c_n are given by

$$\begin{aligned}c_n=&\\&-\frac{\phi_1}{N_n}\Bigg[\int_{\xi_{LS,1}}^{\gamma}\frac{\bar{k}_2\xi-\bar{k}_2\gamma-\xi_{LS,2}}{\bar{k}_2\xi_{LS,1}-\bar{k}_2\gamma-\xi_{LS,2}}\sin\left(\omega_n\left(\xi_{LS,1}-\xi\right)\right)d\xi\\&+\frac{\bar{k}_2}{\bar{\alpha}_2}\int_{\gamma}^{\gamma+\xi_{LS,2}}\frac{\xi-\gamma-\xi_{LS,2}}{\bar{k}_2\xi_{LS,1}-\bar{k}_2\gamma-\xi_{LS,2}}\left(\sin\left(\omega_n\left(\xi_{LS,1}-\gamma\right)\right)\cos\left(\frac{\omega_n(\xi-\gamma)}{\sqrt{\bar{\alpha}_2}}\right)\right.\\&\left.-\frac{\sqrt{\bar{\alpha}_2}}{\bar{k}_2}\cos\left(\omega_n\left(\xi_{LS,1}-\gamma\right)\right)\sin\left(\frac{\omega_n(\xi-\gamma)}{\sqrt{\bar{\alpha}_2}}\right)\right)d\xi\Bigg]\end{aligned} \tag{35}$$

and

$$\begin{aligned}N_n=&\int_{\xi_{LS,1}}^{\gamma}\sin^2\left(\omega_n\left(\xi_{LS,1}-\xi\right)\right)d\xi+\frac{\bar{k}_2}{\bar{\alpha}_2}\int_{\gamma}^{\gamma+\xi_{LS,2}}\Bigg[\sin\left(\omega_n\left(\xi_{LS,1}-\gamma\right)\right)\cos\left(\frac{\omega_n(\xi-\gamma)}{\sqrt{\bar{\alpha}_2}}\right)\\&-\frac{\sqrt{\bar{\alpha}_2}}{\bar{k}_2}\cos\left(\omega_n\left(\xi_{LS,1}-\gamma\right)\right)\sin\left(\frac{\omega_n(\xi-\gamma)}{\sqrt{\bar{\alpha}_2}}\right)\Bigg]^2d\xi\end{aligned} \tag{36}$$

Having determined the temperature distributions in each region, as given by Eqs. (30), (32) and (33), the principle of energy conservation at the two phase change fronts may be used to determine their rates of propagation. This may be shown to result in the following ordinary differential equations that provide explicit expressions for the rates of propagation of the two melting fronts:

$$\begin{aligned}\frac{d\xi_{LS,1}}{d\tau}=&-Ste_1\left(\frac{\partial\theta_{1a}}{\partial\xi}-\frac{\partial\theta_{1b}}{\partial\xi}\right)_{\xi=\xi_{LS,1}}=-Ste_1\Bigg(\frac{\phi_1-1}{\xi_{LS,1}}+\sum_{n=1}^{\infty}\widehat{c}_n\widehat{\omega}_n\cos\left(\widehat{\omega}_n\xi_{LS,1}\right)\\&\exp\left(-\widehat{\omega}_n^2\tau\right)-\frac{\bar{k}_2\phi_1}{\bar{k}_2\xi_{LS,1}-\bar{k}_2\gamma-\xi_{LS,2}}+\sum_{n=1}^{\infty}c_n\omega_n\exp\left(-\omega_n^2\tau\right)\Bigg)\end{aligned} \tag{37}$$

$$\begin{aligned}\frac{d\xi_{LS,2}}{d\tau}=&-\bar{\alpha}_2Ste_2\left(\frac{\partial\theta_{2a}}{\partial\xi}\right)_{\xi=\gamma+\xi_{LS,2}}=-\bar{\alpha}_2Ste_2\Bigg(\frac{\phi_1}{\bar{k}_2\xi_{LS,1}-\bar{k}_2\gamma-\xi_{LS,2}}\\&-\sum_{n=1}^{\infty}c_n\frac{\omega_n}{\sqrt{\bar{\alpha}_2}}\Bigg(\sin\left(\omega_n\left(\xi_{LS,1}-\gamma\right)\right)\sin\left(\frac{\omega_n\xi_{LS,2}}{\sqrt{\bar{\alpha}_2}}\right)+\frac{\sqrt{\bar{\alpha}_2}}{\bar{k}_2}\cos\left(\omega_n\left(\xi_{LS,1}-\gamma\right)\right)\\&\cos\left(\frac{\omega_n\xi_{LS,2}}{\sqrt{\bar{\alpha}_2}}\right)\Bigg)\exp\left(-\omega_n^2\tau\right)\Bigg)\end{aligned} \tag{38}$$

Eqs. (37) and (38), along with initial conditions $\xi_{LS,1}=0$ and $\xi_{LS,2}=0$ at $\tau=0$ may be used to easily determine the locations of the phase change fronts at any time.

Depending on the relative values of parameters such as the Stefan numbers as well as $\bar{\alpha}_2$, ϕ_1 and γ, the melting process of either layer 1 or layer 2 may complete earlier. Therefore, the time at which Stage A finishes may be written as $\tau_A^*=\min(\tau_{1,A}^*,\tau_{2,A}^*)$ where $\tau_{1,A}^*$ and $\tau_{2,A}^*$ are given by the roots of $\xi_{LS,1}(\tau)=\gamma$ and $\xi_{LS,2}(\tau)=1-\gamma$, respectively.

The location of the phase change front in the partially melted layer at the end of Stage A may be written as $\xi_{LS,2A}^*=\xi_{LS,2}(\tau_A^*)$ if layer 1 is fully melted at the end of Stage A (i.e., if $\tau_{1,A}^*<\tau_{2,A}^*$) or $\xi_{LS,1A}^*=\xi_{LS,1}(\tau_A^*)$ in case layer 2 is fully melted at the end of Stage A (i.e., if $\tau_{1,A}^*>\tau_{2,A}^*$).

If layer 1 is fully melted at the end of Stage A, then the initial condition for the next Stage, which is the temperature at the end of Stage A may be written as follows:

$$\theta_{1,A}^*(\xi)=\theta_{1a}(\xi,\tau_A^*)\qquad 0<\xi<\gamma \tag{39}$$

$$\theta_{2,A}^*(\xi)=\begin{cases}\theta_{2a}(\xi,\tau_A^*) & \gamma<\xi<\gamma+\xi_{LS,2A}^*\\ 0 & \gamma+\xi_{LS,2A}^*<\xi<1\end{cases} \tag{40}$$

In contrast, if layer 2 is fully melted at the end of Stage A, then one may write

$$\theta_{1,A}^*(\xi)=\begin{cases}\theta_{1a}(\xi,\tau_A^*) & 0<\xi<\xi_{LS,1A}^*\\ \theta_{1b}(\xi,\tau_A^*) & \xi_{LS,1A}^*<\xi<\gamma\end{cases} \tag{41}$$

$$\theta_{2,A}^*(\xi)=\theta_{2a}(\xi,\tau_A^*)\qquad \gamma<\xi<1 \tag{42}$$

4.2. Stage B: completion of melting of the partially melted layer

Depending on the values of $\tau_{1,A}^*$ and $\tau_{2,A}^*$, one of the two layers remains incompletely melted at end of the Stage A, while the other has melted fully. For example, if $\tau_{1,A}^*<\tau_{2,A}^*$, then layer 1 has melted

completely and some region of layer 2 is not yet melted. Conversely, if $\tau^*_{2,A} < \tau^*_{1,A}$, then layer 2 has melted completely and some region of layer 1 is not yet melted. Since the rest of the phase change process proceeds very differently depending on which layers is not fully melted, therefore, these two cases must be considered separately. This is addressed in the following sub-sections:

4.2.1. Stage B for $\tau^*_{1,A} \le \tau^*_{2,A}$: Completion of melting of layer 2

In this case, layer 1 is fully melted at the start of Stage B. Therefore, during Stage B, layer 1 undergoes sensible temperature rise while heat conducted into layer 2 through layer 1 results in further propagation of the phase change front in layer 2. This problem may be modeled as a recently solved encapsulant-PCM problem [10], in which two non-PCM encapsulants shield a PCM layer from melting. In this case, the temperature field in the first and second encapsulant layers satisfy Eq. (1) in the region $0 < \xi < \gamma$ and Eq. (7) in the region $\gamma < \xi < \gamma + \xi^*_{LS,2A}$. The temperature field in the region in layer 2 that melts during Stage B is also governed by Eq. (7) in the region $\gamma + \xi^*_{LS,2A} < \xi < \gamma + \xi_{LS,2}(\tau)$. The associated boundary and interface conditions are $\theta_1 = 1$ at $\xi = 0$, $\theta_2 = 0$ at $\xi = \gamma + \xi_{LS,2}$, $\theta_1 = \theta_2$ at $\xi = \gamma$ and $\frac{\partial\theta_1}{\partial\xi} = \bar{k}_2\frac{\partial\theta_2}{\partial\xi}$ at $\xi = \gamma$. Similar to the technique used in previous sections, the temperature distribution in this case can be derived as follows:

$$\theta_1(\xi,\tau) = 1 - \frac{\bar{k}_2\xi}{\bar{k}_2\gamma + \xi_{LS,2}} + \sum_{n=1}^{\infty} c_n \sin(\omega_n\xi)\exp\left(-\omega_n^2(\tau-\tau^*_A)\right) \tag{43}$$

$$\theta_2(\xi,\tau) = \frac{\gamma+\xi_{LS,2}-\xi}{\bar{k}_2\gamma+\xi_{LS,2}} + \sum_{n=1}^{\infty} c_n\left(\sin(\omega_n\gamma)\cos\left(\frac{\omega_n(\xi-\gamma)}{\sqrt{\bar{\alpha}_2}}\right) + \frac{\sqrt{\bar{\alpha}_2}}{\bar{k}_2}\cos(\omega_n\gamma)\sin\left(\frac{\omega_n(\xi-\gamma)}{\sqrt{\bar{\alpha}_2}}\right)\right)\exp\left(-\omega_n^2(\tau-\tau^*_A)\right) \tag{44}$$

where the eigenvalues ω_n satisfy

$$\cot\left(\frac{x\xi_{LS,2}}{\sqrt{\bar{\alpha}_2}}\right) + \frac{\sqrt{\bar{\alpha}_2}}{\bar{k}_2}\cot(x\gamma) = 0 \tag{45}$$

and the coefficients c_n are given by

$$c_n = -\frac{1}{N_n}\left[\int_0^{\gamma}\left(\theta^*_{1,A}(\xi) - 1 + \frac{\bar{k}_2\xi}{\bar{k}_2\gamma+\xi_{LS,2}}\right)\sin(\omega_n\xi)d\xi + \frac{\bar{k}_2}{\bar{\alpha}_2}\int_{\gamma}^{\gamma+\xi_{LS,2}}\left(\theta^*_{2,A}(\xi) - \frac{\gamma+\xi_{LS,2}-\xi}{\bar{k}_2\gamma+\xi_{LS,2}}\right)\left[\sin(\omega_n\gamma)\cos\left(\frac{\omega_n(\xi-\gamma)}{\sqrt{\bar{\alpha}_2}}\right) + \frac{\sqrt{\bar{\alpha}_2}}{\bar{k}_2}\cos(\omega_n\gamma)\sin\left(\frac{\omega_n(\xi-\gamma)}{\sqrt{\bar{\alpha}_2}}\right)\right]d\xi\right] \tag{46}$$

and

$$N_n = \int_0^{\gamma}\sin^2(\omega_n\xi)d\xi + \frac{\bar{k}_2}{\bar{\alpha}_2}\int_{\gamma}^{\gamma+\xi_{LS,2}}\left[\sin(\omega_n\gamma)\cos\left(\frac{\omega_n(\xi-\gamma)}{\sqrt{\bar{\alpha}_2}}\right) + \frac{\sqrt{\bar{\alpha}_2}}{\bar{k}_2}\cos(\omega_n\gamma)\sin\left(\frac{\omega_n(\xi-\gamma)}{\sqrt{\bar{\alpha}_2}}\right)\right]^2 d\xi \tag{47}$$

As a result, an expression for the rate of phase change front propagation can be written as

$$\frac{d\xi_{LS,2}}{d\tau} = -\bar{\alpha}_2 Ste_2\left(\frac{\partial\theta_2}{\partial\xi}\right)_{\xi=\gamma+\xi_{LS,2}} = \bar{\alpha}_2 Ste_2\left(\frac{-1}{\bar{k}_2\gamma+\xi_{LS,2}} + \sum_{n=1}^{\infty} c_n\frac{\omega_n}{\sqrt{\bar{\alpha}_2}}\left(-\sin(\omega_n\gamma)\sin\left(\frac{\omega_n\xi_{LS,2}}{\sqrt{\bar{\alpha}_2}}\right) + \frac{\sqrt{\bar{\alpha}_2}}{\bar{k}_2}\cos(\omega_n\gamma)\cos\left(\frac{\omega_n\xi_{LS,2}}{\sqrt{\bar{\alpha}_2}}\right)\right)\exp\left(-\omega_n^2(\tau-\tau^*_A)\right)\right) \tag{48}$$

along with the initial condition $\xi_{LS,2}(\tau^*_A) = \xi^*_{LS,2A}$.

In this case, Stage B, and therefore, the entire melting process is complete when the melting front in the second layer reaches the end of the geometry, i.e., at $\tau = \tau^*_B$ where $\xi_{LS,2}(\tau^*_B) = 1 - \gamma$.

4.2.2. Stage B for $\tau^*_{2,A} \le \tau^*_{1,A}$: Completion of melting of layer 1

This sub-section considers a scenario where the melting of layer 2 occurs faster than that of layer 1 during Stage A. As a result, in this case, layer 2 has already melted by the end of Stage A, and in Stage B, the phase change propagation front in the first layer grows until all of layer 1 has also melted.

This problem may be modeled as a three-layer diffusion problem along with phase change propagation in the first layer. Heat diffusion from the hot wall through the first layer results in further melting, and, in addition, there is heat transfer from the phase change front into the other two layers as well. For convenience, the melted and unmelted regions in layer 1 are denoted as 1a and 1b, respectively, whereas layer 2 forms the third layer in this problem. The temperature fields in regions 1a and 1b satisfy Eq. (1) in $0 < \xi < \xi_{LS,1}$ and $\xi_{LS,1} < \xi < \gamma$, respectively. The temperature field in the region in layer 2 satisfies Eq. (7) in the region $\gamma < \xi < 1$. The associated boundary and interface conditions are $\theta_{1a} = 1$ at $\xi = 0$, $\theta_{1a} = \phi_1$ at $\xi = \xi_{LS,1}$, $\theta_{1b} = \phi_1$ at $\xi = \xi_{LS,1}$, $\theta_{1b} = \theta_2$ at $\xi = \gamma$, $\frac{\partial\theta_{1b}}{\partial\xi} = \bar{k}_2\frac{\partial\theta_2}{\partial\xi}$ at $\xi = \gamma$ and $-\bar{k}_2\frac{\partial\theta_2}{\partial\xi} = Bi\cdot\theta_2$ at $\xi = 1$. Similar to the technique used in previous sections, the temperature distribution in layer 1a case can be derived as follows:

$$\theta_{1a}(\xi,\tau) = 1 - \frac{1-\phi_1}{\xi_{LS,1}}\xi + \sum_{n=1}^{\infty}\hat{c}_n\sin(\hat{\omega}_n\xi)\exp\left(-\hat{\omega}_n^2(\tau-\tau^*_A)\right) \tag{49}$$

where $\hat{\omega}_n = \frac{n\pi}{\xi_{LS,1}}$ and coefficients $\hat{c}_n$ are obtained using orthogonality as follows:

Table 2
Values of thermophysical properties of the two PCMs used in this work [35,36].

	Octadecane	Eicosane
Thermal conductivity, $Wm^{-1}K^{-1}$	0.25	0.15
Heat capacity, $Jkg^{-1}K^{-1}$	2300	2210
Density, kgm^{-3}	780	785
Latent heat, Jkg^{-1}	244,000	247,000
Phase change temperature, °C	28	36

$$\widehat{c}_n = \frac{2}{\xi_{LS,1}} \int_0^{\xi_{LS,1}} \left(\theta^*_{1,A}(\xi) - \left(1 - (1-\phi_1)\frac{\xi}{\xi_{LS,1}} \right) \right) \sin(\widehat{\omega}_n \xi) d\xi \tag{50}$$

The temperature fields in the other two regions are coupled to each other through the interface conditions. By solving a two-layer diffusion problem for these regions using techniques similar to the one discussed in Section 3, the following expressions for the temperature fields in layers 1 and 2 may be derived.

$$\theta_{1b}(\xi,\tau) = \frac{\phi_1(-Bi\bar{k}_2\xi + Bi + \bar{k}_2 - Bi\gamma + Bi\gamma\bar{k}_2)}{Bi + \bar{k}_2 - Bi\gamma + Bi\gamma\bar{k}_2 - Bi\bar{k}_2\xi_{LS,1}} + \sum_{n=1}^{\infty} c_n \sin(\omega_n(\xi_{LS,1} - \xi)) \exp(-\omega_n^2(\tau - \tau^*_A)) \tag{51}$$

$$c_n = \frac{1}{N_n} \left[\int_{\xi_{LS,1}}^{\gamma} \left(\theta^*_{1,A}(\xi) - \frac{\phi_1(-Bi\bar{k}_2\xi + Bi + \bar{k}_2 - Bi\gamma + Bi\gamma\bar{k}_2)}{Bi + \bar{k}_2 - Bi\gamma + Bi\gamma\bar{k}_2 - Bi\bar{k}_2\xi_{LS,1}} \right) \sin(\omega_n(\xi_{LS,1} - \xi)) d\xi + \frac{\bar{k}_2}{\bar{\alpha}_2} \int_{\gamma}^{1} \left(\theta^*_{2,A}(\xi) - \frac{\phi_1(-Bi\xi + Bi + \bar{k}_2)}{Bi + \bar{k}_2 - Bi\gamma + Bi\gamma\bar{k}_2 - Bi\bar{k}_2\xi_{LS,1}} \right) \left(\sin(\omega_n(\xi_{LS,1} - \gamma)) \cos\left(\frac{\omega_n(\xi - \gamma)}{\sqrt{\bar{\alpha}_2}} \right) - \frac{\sqrt{\bar{\alpha}_2}}{\bar{k}_2} \cos(\omega_n(\xi_{LS,1} - \gamma)) \sin\left(\frac{\omega_n(\xi - \gamma)}{\sqrt{\bar{\alpha}_2}} \right) \right) d\xi \right] \tag{54}$$

and

$$N_n = \int_{\xi_{LS,1}}^{\gamma} \sin^2(\omega_n(\xi_{LS,1} - \xi)) d\xi + \frac{\bar{k}_2}{\bar{\alpha}_2} \int_{\gamma}^{1} \left(\sin(\omega_n(\xi_{LS,1} - \gamma)) \cos\left(\frac{\omega_n(\xi - \gamma)}{\sqrt{\bar{\alpha}_2}} \right) - \frac{\sqrt{\bar{\alpha}_2}}{\bar{k}_2} \cos(\omega_n(\xi_{LS,1} - \gamma)) \sin\left(\frac{\omega_n(\xi - \gamma)}{\sqrt{\bar{\alpha}_2}} \right) \right)^2 d\xi \tag{55}$$

$$\theta_2(\xi,\tau) = \frac{\phi_1(-Bi\xi + Bi + \bar{k}_2)}{Bi + \bar{k}_2 - Bi\gamma + Bi\gamma\bar{k}_2 - Bi\bar{k}_2\xi_{LS,1}} + \sum_{n=1}^{\infty} c_n \left(\sin(\omega_n(\xi_{LS,1} - \gamma)) \cos\left(\frac{\omega_n(\xi - \gamma)}{\sqrt{\bar{\alpha}_2}} \right) - \frac{\sqrt{\bar{\alpha}_2}}{\bar{k}_2} \cos(\omega_n(\xi_{LS,1} - \gamma)) \sin\left(\frac{\omega_n(\xi - \gamma)}{\sqrt{\bar{\alpha}_2}} \right) \right) \exp(-\omega_n^2(\tau - \tau^*_A)) \tag{52}$$

where the eigenvalues ω_n satisfy

$$\sin(x(\xi_{LS,1} - \gamma)) \left(\cos\left(\frac{x(1-\gamma)}{\sqrt{\bar{\alpha}_2}} \right) - \frac{\bar{k}_2 x}{Bi\sqrt{\bar{\alpha}_2}} \sin\left(\frac{x(1-\gamma)}{\sqrt{\bar{\alpha}_2}} \right) \right) - \frac{\sqrt{\bar{\alpha}_2}}{\bar{k}_2} \cos(x(\xi_{LS,1} - \gamma)) \left(\sin\left(\frac{x(1-\gamma)}{\sqrt{\bar{\alpha}_2}} \right) + \frac{\bar{k}_2 x}{Bi\sqrt{\bar{\alpha}_2}} \cos\left(\frac{x(1-\gamma)}{\sqrt{\bar{\alpha}_2}} \right) \right) = 0 \tag{53}$$

and the coefficients c_n are given by

Thus, the rate of phase change front propagation is given by

$$\frac{d\xi_{LS,1}}{d\tau} = -Ste_1 \left(\frac{\partial\theta_{1a}}{\partial\xi} - \frac{\partial\theta_{1b}}{\partial\xi} \right)_{\xi=\xi_{LS,1}} = -Ste_1 \left(\frac{\phi_1 - 1}{\xi_{LS,1}} + \sum_{n=1}^{\infty} \widehat{c}_n \widehat{\omega}_n \cos(\widehat{\omega}_n \xi_{LS,1}) \exp(-\widehat{\omega}_n^2(\tau - \tau^*_A)) + \frac{Bi\bar{k}_2\phi_1}{Bi + \bar{k}_2 - Bi\gamma + Bi\gamma\bar{k}_2 - Bi\bar{k}_2\xi_{LS,1}} + \sum_{n=1}^{\infty} c_n \omega_n \exp(-\omega_n^2(\tau - \tau^*_A)) \right) \tag{56}$$

with the initial condition $\xi_{LS,1}(\tau^*_A) = \xi^*_{LS,1A}$.

In this case, Stage B, and therefore, the entire melting process is complete when the melting front in the first layer reaches the interface between layers, i.e., at $\tau = \tau^*_B$ where $\xi_{LS,1}(\tau^*_B) = \gamma$. This marks the end of the entire melting process in the two-layer geometry from Case II.

A summary of governing equations and equations that describe the temperature field and phase change front location during each Stage for

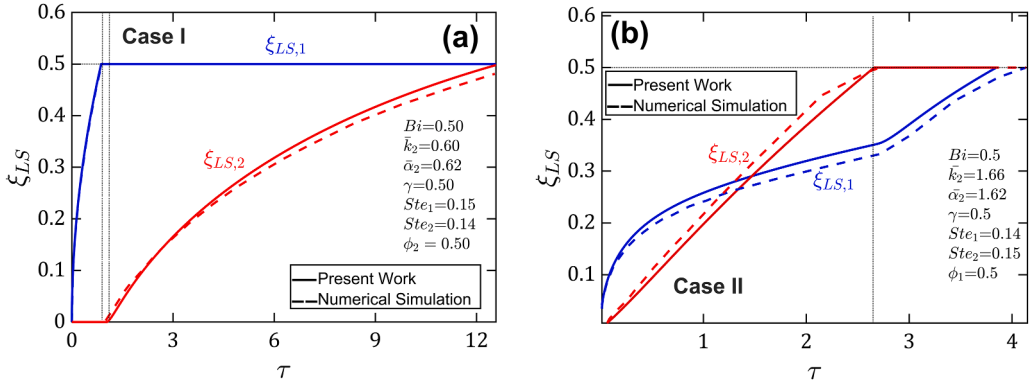

Fig. 2. Comparison of the analytical model with finite-element simulations: Phase change front locations in both layers as functions of time. (a) Lower-melting PCM adjacent to heat source (Case I), (b) Higher-melting PCM adjacent to heat source (Case II). PCMs are taken to be octadecane and eicosane, with a 44 °C temperature on the hot wall. Results from finite-element simulations are shown for comparison.

this Case is presented in Table 1.

5. Results and discussion

This section discusses key results based on the theoretical model presented in previous sections. First, verification of the theoretical model by comparison with numerical simulations is presented. This is followed by discussion of typical melting front propagation and temperature distribution plots. The practically important question of the total time for melting is addressed. This includes a discussion of conditions in which both layers may finish melting simultaneously. This is followed by a discussion of the effect of Stefan numbers on the melting process.

5.1. Verification

In order to verify the analytical models presented in Sections 2–4, results for representative problems are first compared with independent finite-element simulations carried out in ANSYS-CFX. For this purpose, both materials are modeled as mixtures of solid and liquid phases with a certain mixture fraction that varies over space and time. The simulation sets up computation of the mixture fraction distribution in addition to the temperature distribution at multiple times, thereby determining how the phase change front propagates with time. Mesh size and timestep are both refined until further refinement does not result in appreciable changes in the computed temperature field. Locations of the two phase change fronts are determined at each timestep by tracking the location at which the volume fraction of solid phase changes from 1 to 0.

A comparison is carried out for the melting of a two-layer body comprising octadecane and eicosane of thicknesses 5.0 mm each, being heated up from one side by a 44 °C external temperature. Values of thermophysical properties of the two PCMs are taken from past literature [35,36] and are summarized in Table 2. Notably, octadecane melts at a lower temperature than eicosane. The Biot number representing the convective heat transfer boundary condition at the right end of the geometry is taken to be 0.5. All non-dimensional parameters used in the analytical model are computed on the basis of the dimensional problem described above. Fig. 2 presents a comparison between the analytical model and simulations in terms of the locations of the two melting fronts as functions of time. Plots are presented in non-dimensional form. Boundaries between sucessive Stages are indicated by vertical lines. Fig. 2(a) presents this comparison for the case where the lower-melting octadecane is placed next to the heat source, corresponding to Case I (Section 3). The opposite case, in which the higher-melting eicosane is placed next to the heat source, corresponding to Case II (Section 4) is presented in Fig. 2(b). In both cases, there is very good agreement between the analytical model and finite-element simulations. In Case I presented in Fig. 2(a), the model is able to successfully capture the melting of layer 1 first (Stage A), followed by sensible heating of both layers with no propagation of the melting front (Stage B), during which, neither $\xi_{LS,1}$ nor $\xi_{LS,2}$ change with time, and, finally, the melting of layer 2 (Stage C). For the parameter values used here, Stage B is found be very brief. Similarly, in Case II presented in Fig. 2(b), the model is able to successfully capture the simultaneous melting of both layers at early times and completion of melting of layer 2 first (Stage A), followed by the melting of the remainder of layer 1 (Stage B).

Further verification of the theoretical model is carried out by comparing the predicted temperature distributions at multiple times with numerical simulations. Both Cases I and II are considered. For the same set of problem parameters as Fig. 2 above, Figs. 3(a) and 3(b) present this comparison for Cases I and II, respectively. In each case, the temperature distribution is plotted at two times in different Stages of the phase change process and compared with numerical simulations. There is, in general, very good agreement between the two. The agreement is nearly exact for Case I at $\tau = 0.5$, which lies in Stage A of this Case. This is because Stage A of Case I is governed by the exact analytical solution of the Stefan problem in layer 1, whereas layer 2 does not commence melting in this Stage. At other times, several factors likely contribute towards the small disagreement between the theoretical model and numerical simulations. These include the approximate nature of the theoretical model, as well as discretization and other computational errors in the numerical simulations. The good agreement in general with finite-element simulations shown in Figs. 2 and 3 for both cases considered here provide confidence in the accuracy of the analytical model presented in this work.

Further verification of the theoretical model developed here is carried out by considering the special case in which both layers have the same thermophysical properties. In such a case, assuming both layers are initially at the melting temperature, this problem is expected to reduce to the standard one-layer Stefan problem with constant temperature boundary condition, for which, an analytical solution is available [2]. A comparison of the predictions of the theoretical model with the Stefan solution is presented in Fig. 4. Two different values of the Stefan number are considered. As expected, there is exact agreement in Stage A of the melting process, during which, the theoretical model developed here is based on the Stefan solution. Afterwards, there is a minor deviation between the two curves, which is attributed to the approximate nature of the analytical technique used here. As expected, the deviation is greater at the larger value of *Ste* considered for this comparison. Nevertheless, the good agreement in general indicates that the theoretical model developed in this work agrees well with the Stefan solution when both layers have the same thermophysical properties.

5.2. Melting front propagation and temperature distributions

Representative two-PCM melting problems are solved using the

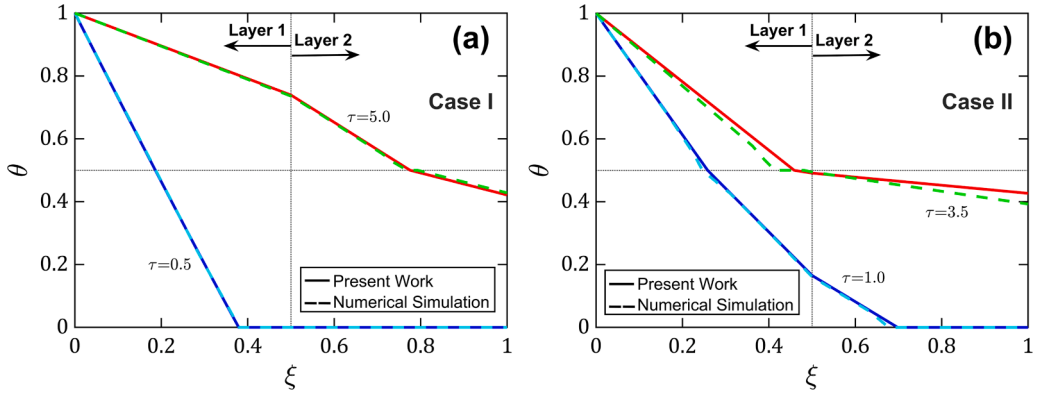

Fig. 3. Comparison of the analytical model with finite-element simulations: Temperature distribution in both layers at two different times for the problem considered in Fig. 2. (a) Case I, (b) Case II. Results from finite-element simulations are shown for comparison.

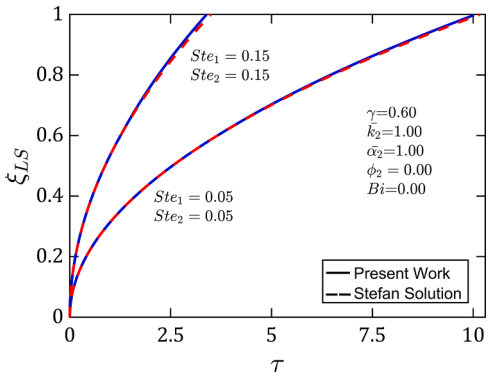

Fig. 4. Comparison of the theoretical model with the Stefan solution in the case of identical properties of both layers, along with $Bi = 0$. Comparison is presented for two different values of the Stefan number.

analytical model presented in Section 2–4. Similar to the previous subsection, octadecane and eicosane are also considered as the two PCMs in this analysis. The hot wall temperature that drives phase change is taken to be 44 °C. Results pertaining to the problem in which the lower-melting PCM is placed next to the hot wall (Case I presented in Section 3) are discussed next, followed by discussion of the problem in which the higher-melting PCM is placed next to the hot wall (Case II discussed in Section 4).

5.2.1. Case I

For this case, the second layer is taken to be four times as thick as the first one, so that $\gamma = 0.8$. For the first scenario, in which octadecane is placed next to the hot wall, the melting fronts $\xi_{LS,1}$ and $\xi_{LS,2}$ are plotted as functions of time in Fig. 5. As expected, due to the lower melting temperature of the first layer, in this case, layer 1 is found to start melting immediately, whereas layer 2 does not. Melting of layer 1 slows down over time due to the well-known shielding of the hot source by the already melted liquid in this Stefan problem. Stage A proceeds until $\tau = \tau_A^*$, when all of layer 1 has melted, at which point, $\xi_{LS,1} = \gamma$ while $\xi_{LS,2}$ is still zero. Afterwards, as discussed in Section 3.2, there is no melting during Stage B, represented by flat $\xi_{LS,1}$ and $\xi_{LS,2}$ curves between $\tau = \tau_A^*$ and $\tau = \tau_B^*$, depicted by dotted vertical lines. After a short Stage B, layer 2 proceeds to melt during Stage C, and the $\xi_{LS,2}$ curve rises while $\xi_{LS,1}$ remains flat. The entire melting process finishes at $\tau = \tau_{total}$, when $\xi_{LS,2}$ becomes equal to $1 - \gamma$. For this case, the numerical values of τ_A^*, τ_B^* and τ_{total} are found to be 2.23, 2.53 and 8.33, respectively.

Note that in this case, the two layers melt in series, and, therefore, layer 2 will always finish melting later than layer 1. From a practical perspective, it is of interest to investigate the conditions in which the two layers may finish melting at the same time. This is possible under a special case in Case II, which is discussed in more detail in subsequent sub-sections.

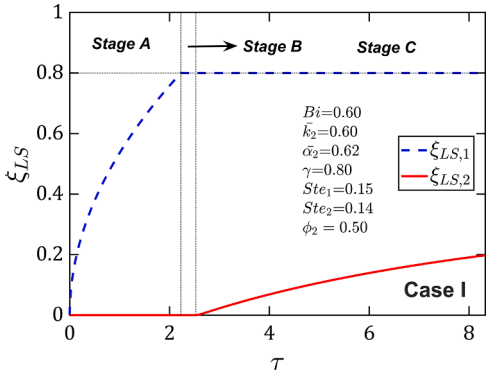

Fig. 5. Phase change locations in both layers as functions of time for Case I (lower-melting PCM adjacent to heat source). Parameter values are: $\gamma = 0.80$, $Ste_1 = 0.15$, $Ste_2 = 0.14$, $\bar{\alpha}_2 = 0.62$, $\bar{k}_2 = 0.60$, $Bi = 0.60$, $\phi_2 = 0.50$.

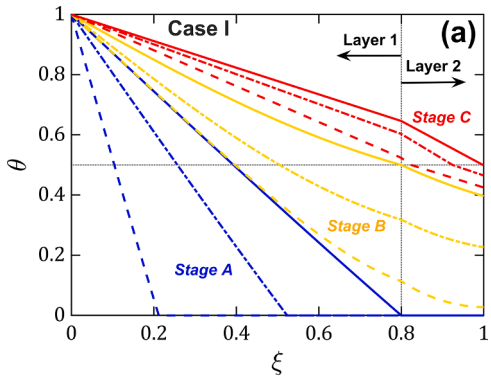

Fig. 6. Temperature distributions at three different times, each during stages A, B and C of the melting process shown in Fig. 5 (Case I). Layer thicknesses and melting point of the second layer are shown as vertical and horizontal dotted lines, respectively. The times shown, from left to right are $\tau = 0.16,\ 0.95,\ 2.23,\ 2.25,\ 2.35,\ 2.53,\ 3.02,\ 5.52$ and 8.33.

In order to illustrate the evolution of the temperature field with time in Case I, temperature distributions within both layers are plotted at three successive times during Stages A, B and C in Fig. 6 for the same set of parameters as the previous Figure. These plots show that layer 1 ($\xi < \gamma$) undergoes melting and subsequent sensible heating during Stage A. There is no melting or even sensible heating of layer 2 ($\xi > \gamma$) during Stage A because the melting front has not yet reached the interface between the layers. Even after this occurs at $\tau = \tau_A^*$, there is still no melting of layer 2 in Stage B because the temperature remains below the melting temperature of layer 2, ϕ_2 shown by a dotted horizontal line. Stage B curves in Fig. 6 show only sensible temperature rise in both layers, consistent with flat $\xi_{LS,1}$ and $\xi_{LS,2}$ curves shown in Fig. 5 during this period. This continues until temperature at the interface, $\xi_{LS,1} = \gamma$ shown by the dotted vertical line in Fig. 6, reaches the melting temperature ϕ_2. Finally, during Stage C, it is found that temperature in a portion of layer 2 rises above its melting temperature ϕ_2 as the melting front $\xi_{LS,2}$ propagates until, finally, at $\tau = \tau_{total}$, all of layer 2 has melted and temperature at the far end, $\xi = 1$ becomes ϕ_2.

Taken together, Figs. 5 and 6 illustrate several key characteristics of temperature distribution and melting front propagation in both layers for Case I where the lower melting material, octadecane in this case, is placed next to the hot source.

Discussion of the melting process for Case II, in which the higher melting PCM is placed next to the hot source instead is presented next.

5.2.2. Case II

The same set of problem parameters as Section 5.2.1 are considered again, including thermophysical properties of the two PCMs. However, in this case, the higher melting PCM is placed next to the hot source. Melting front propagation plots for two different relative thicknesses $\gamma = 0.2$ and $\gamma = 0.6$ are presented in Figs. 7(a) and 7(b), respectively. Temperature distributions in both layers are plotted at different times for these thicknesses in Figs. 8(a) and 8(b).

As discussed in Section 4, placing the higher-melting eicosane next to the heat source results in the simultaneous onset of melting in both layers starting at $\tau = 0$, which is confirmed by both Figs. 7(a) and 7(b). It is found, as expected, that the initial rate of melting is greater in layer 1, which is located directly next to the heat source. Over time, however, the rate of melting in layer 2 also rises and catches up with layer 1. Phase change and sensible heating occur in both layers during Stage A. For $\gamma = 0.2$, it is found that temperature at the interface, $\xi = \gamma$ reaches the layer 1 melting point ϕ_1 before layer 2 melts completely. Therefore, layer 1

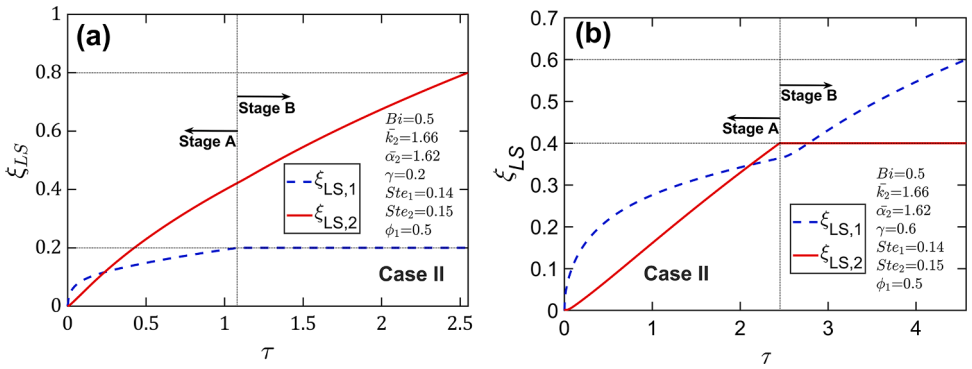

Fig. 7. Phase change front locations in both layers as functions of time for Case II (higher-melting PCM adjacent to heat source). (a) and (b) present results for $\gamma = 0.2$ and $\gamma = 0.6$, respectively, for which the first and second layers, respectively, finish melting first. Other parameter values are: $Ste_1 = 0.14$, $Ste_2 = 0.15$, $\bar{\alpha}_2 = 1.62$, $\bar{k}_2 = 1.66$, $Bi = 0.50$, $\phi_1 = 0.50$. Layer thicknesses and melting point of the first layer are shown as vertical and horizontal dotted lines, respectively.

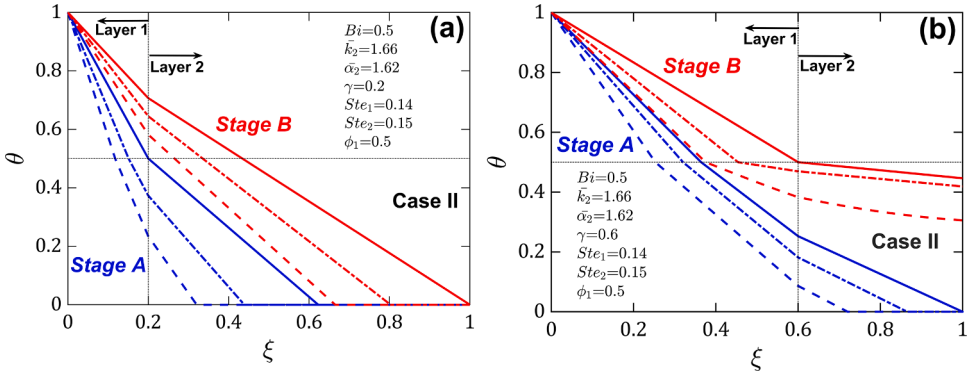

Fig. 8. Temperature distributions at three different times each during Stages A and B of a Case II melting process. Results are presented for (a) $\gamma = 0.2$ and (b) $\gamma = 0.6$ that result in earlier completion of melting of first and second layer, respectively. Other parameters used here correspond to Fig. 7. Interface between layers and melting point of the first layer are shown as vertical and horizontal dotted lines, respectively. The times shown, from left to right, are (a) $\tau = 0.24,\ 0.52,\ 1.08,\ 1.22,\ 1.71$, and 2.55, (b) $\tau = 0.77,\ 1.61,\ 2.45,\ 2.59,\ 3.17$ and 4.57.

finishes its melting process first, as shown at $\tau = \tau_A^*$ indicated by a vertical dotted line in Fig. 7(a), marking the end of Stage A. Subsequently, during Stage B, the $\xi_{LS,1}$ plot stays flat, since the melting of layer 1 is already complete, whereas the $\xi_{LS,2}$ plot continues to rise due to continued melting of layer 2 during Stage B. Eventually, at $\tau = \tau_{total}$, all of layer 2 also melts and the process is complete. The temperature plots at different times during both stages shown in Fig. 8(a) are consistent with the melting front propagation shown in Fig. 7(a). Specifically, Fig. 8(a) shows temperature rise above melting temperature for both layers during Stage A, followed by continued temperature rise in both layers and the melting of layer 2 during Stage B until the $\xi_{LS,2}$ front reaches the end of layer 2, indicating completion of the melting process.

In contrast, in the $\gamma = 0.6$ case, in which, layer 1 is relatively thicker, the melting process of layer 2 finishes first, as shown in Fig. 7(b). In this case, due to the relatively thinner layer 2, the melting front in layer 2 first reaches the far end ($\xi_{LS,2} = 1 - \gamma$), indicating completion of melting in layer 2 before layer 1. As shown in Fig. 7(b), at the time when $\xi_{LS,2} = 1 - \gamma$, i.e., completion of melting of layer 2, the value of $\xi_{LS,1}$ is still less than γ. The remainder of layer 1 completes its melting in Stage B, during which, temperatures in both layers continue to rise, as shown in Fig. 8 (b), and $\xi_{LS,1}$ continues to grow while $\xi_{LS,2}$ remains constant, as shown in Fig. 7(b). This continues until $\xi_{LS,1}$ reaches a value of γ, at which time, the melting process is complete. Fig. 7(b) shows that once layer 2 has completely melted, the rate of melting of layer 1 increases, because now all the heat supplied can be used for melting only layer 1. Also, in Fig. 8 (b), it may be noted that the value and slope of the temperature distribution at $\xi = 1$ during Stage B is determined by the Biot number defined at that boundary.

Note that layer 2 melts faster in the $\gamma = 0.6$ case despite being farther from the heat source because of its lower melting point and relatively lower thickness in this case. Between the two cases presented in Figs. 7 (a) and 7(b), there is likely to exist a certain relative layer thickness γ, at which, both layers finish melting simultaneously. This is analyzed in more detail in a subsequent sub-section.

The plots presented in this sub-section illustrate the key phase change propagation and temperature rise phenomena based on a systematic analysis of melting and sensible heating of both layers presented in Section 2. The evolution of the temperature fields as well as melting front propagation with time presented in these plots are consistent with the physical understanding of phase change heat transfer, particularly in cases where the material being melted is shielded by material that is already melted or is not yet ready to melt due to being supercooled. Based on the plots presented in this section, it is also possible to determine system performance parameters such as total time to melt and total energy absorbed, as well as to determine which of the two layers will finish melting first. An analysis of such system performance parameters is presented next.

5.3. Total time for completion of melting

The total time taken for completion of melting is an important performance parameter in practical energy storage problems. Often, only a limited amount of time is available for heat transfer and energy storage in the PCMs, and, therefore, the two-PCM stack must be designed in order that the time taken for complete melting be as close as possible to the time available. If the time taken for complete melting is much larger, then the system is overdesigned and a large part of the PCM is not being

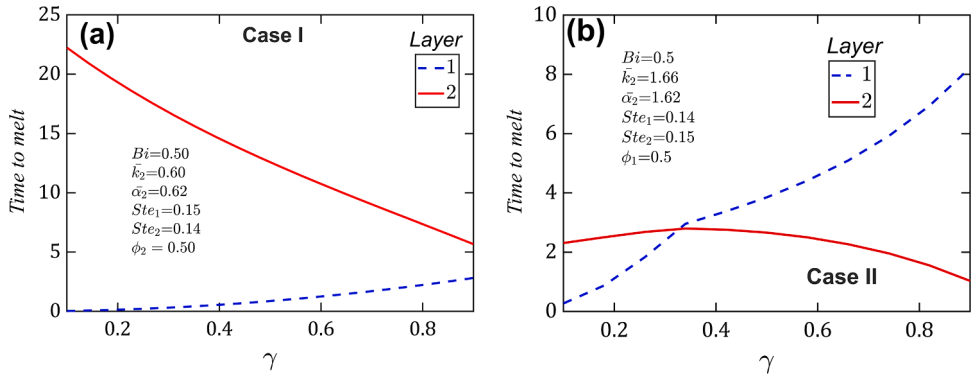

Fig. 9. Effect of the interface location on melting process: Time for total melting for each layer as functions of relative layer thickness γ. (a) Case I, (b) Case II. Other problem parameters correspond to Figs. 5 and 6, respectively.

used for energy storage. On the other hand, if the time taken for complete melting is much smaller, then the system fails to store much of the available energy in latent form, thereby limiting the effectiveness of latent heat storage.

In order to demonstrate the capability of the analytical model presented here to answer these important design questions, the time taken for melting of the two layers is analyzed as a function of various problem parameters. For Case I (lower-melting PCM placed next to the heat source), Fig. 9(a) plots the time at which each of the two layers melt as functions of the relative layer thickness γ. In this case, the layer 2 curve also represents the total time taken for complete melting since layer 2 always melts later than layer 1. As γ increases, the time taken for layer 1 to melt increases, due to greater relative thickness of layer 1, whereas the time taken for layer 2 to melt reduces. As expected, layer 1 is found to always melt earlier than layer 2, even when layer 1 is very thin (large γ) because in this Case, layer 1 has a lower melting temperature, and, therefore, layer 2 cannot begin to melt until all of layer 1 has melted. In other words, decreasing layer 2 thickness reduces total melting time, since layer 2 has a higher melting temperature in this case.

Fig. 9(b) presents a similar analysis for Case II, in which, the lower-melting PCM is placed away from the hot source. In this case, as γ increases starting from a small value, both layers first take longer to melt. The rate of increase of τ_{total} with γ for layer 1 is particularly steep because of the increased thickness of layer 1 with increasing γ. However, unlike Case I shown in Fig. 9(a), in this case, the time taken for layer 2 to melt also increases slightly with increasing γ, because of the increased resistance to heat flow to layer 2 through layer 1. This is, however, only a weak effect. At a certain layer thickness, $\gamma = 0.33$, in this case, the two curves in Fig. 9(b) are found to intersect, indicating that both layers finish melting at the same time, which is indeed a favorable outcome as

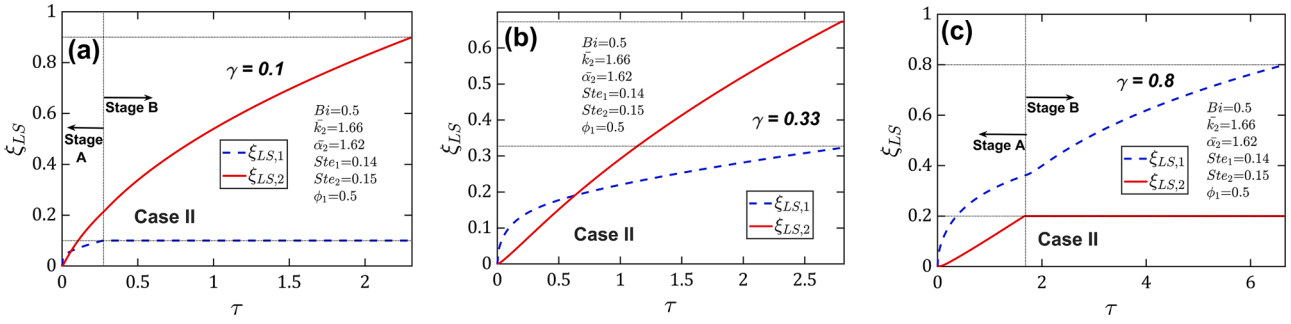

Fig. 10. Phase change front locations in both layers as functions of time for the Case II process considered in Fig. 9(b) for three different values of relative layer thickness γ, including a case where both layers finish melting at the same time. Other parameter values are: $Ste_1 = 0.14$, $Ste_2 = 0.15$,$\bar{\alpha}_2 = 1.62$,$\bar{k}_2 = 1.66$, $Bi = 0.50$, $\phi_1 = 0.50$.

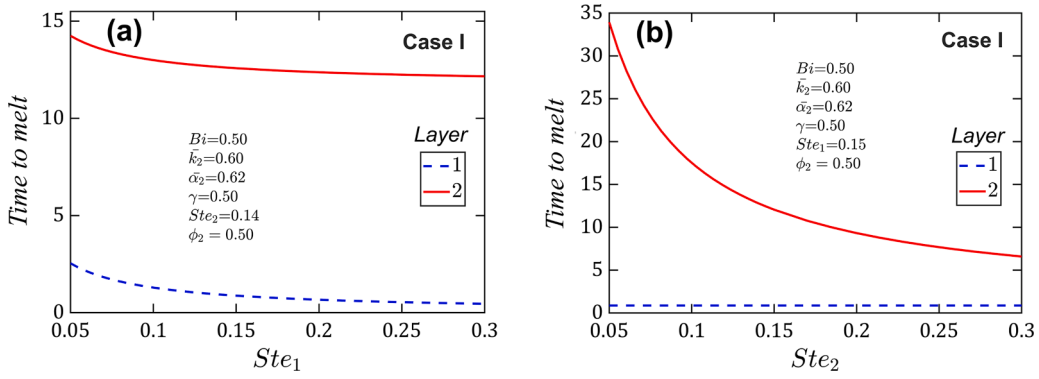

Fig. 11. Effect of Stefan numbers: Total melting time for each layer in Case I as functions of (a) Ste_1 (with $Ste_2 = 0.14$); (b) Ste_2 (with $Ste_1 = 0.15$). Other problem parameters correspond to Figs. 5 and 7, respectively.

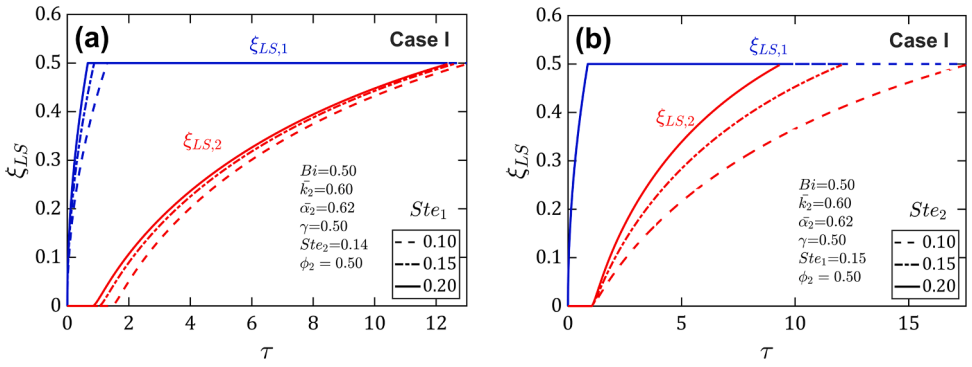

Fig. 12. Phase change front locations in both layers as functions of time for Case I process for three different values of (a) Ste_1 (with $Ste_2 = 0.14$); b) Ste_2 (with $Ste_1 = 0.15$). Other parameter values are: $\gamma = 0.50$, $\bar{\alpha}_2 = 0.62, \bar{k}_2 = 0.60$, $Bi = 0.50$, $\phi_2 = 0.50$.

it fully utilizes the latent heat storage capability of both layers. Making layer 1 thicker than this optimal value results in increased time taken to melt layer 1 and a relatively weaker reduction in time taken for layer 2 to melt. Note that the greater of the two curves in Fig. 9(b) represents the total time to melt. Further, note that the nature of curve in Fig. 9(b) at small γ is different from that at large γ, with the crossover occurring around $\gamma = 0.33$. This is because for small values of γ, layer 1 finishes melting first, and, therefore, its melting time is governed primarily by Stage A of this Case, determined by the equations given in Section 4.1. On the other hand, for large values of γ, layer 2 finishes melting first and, therefore, the rest of the melting of layer 1 and its total time to melt is governed by an entirely different set of equations, given in Section 4.2.2. Results presented in Fig. 9(b) for Case II are supplemented with melting front propagation plots for three different values of relative layer thickness γ in Fig. 10. The thicknesses of the two layers, γ and $1 - \gamma$, respectively, are indicated as dotted horizontal lines. As shown in Fig. 10 (a), when γ is small, i.e., layer 2 is relatively thicker, and thus, layer 1 melts much faster, while completion of melting of layer 2 occurs much later. In contrast, when γ is much larger, as shown in Fig. 10(c), layer 2 finishes melting first and $\xi_{LS,2}$ remains flat afterwards while layer 1 finishes melting. Between these two extremes, there exists an intermediate value of γ, at which, the melting processes in both layers exactly balance each other, so that the phase change fronts in both layers reach their respective ends ($\xi_{LS,1} = \gamma$ and $\xi_{LS,2} = 1 - \gamma$) at nearly the same time. This case, shown in Fig. 10(b), is the most favorable as it leads to the complete utilization of the latent heat storage capacity of both layers within the same timeframe. It must be noted that this particular case has no Stage B associated with it, as the entire melting completes during Stage A. Figs. 9(b) and 10 demonstrate the capability of the analytical model to predict such optimal configurations in two-PCM problems.

5.4. Impact of Stefan numbers

Stefan number is the key non-dimensional parameter that governs the nature of melting and solidification processes [1,2]. In addition to the externally imposed temperature at the boundary, the Stefan number also includes the heat capacity and latent heat of the material. Due to the presence of two distinct materials, the problem considered here contains two independent Stefan numbers. In order to understand the impact of the Stefan numbers on melting characteristics, the time taken for melting for both layers is plotted as a function of Ste_1 and Ste_2 in Fig. 11 for Case I, with the same set of parameter values as Fig. 2(a). It is found that increasing Ste_1 (while holding Ste_2 constant reduces the melting time for both layer 1 and layer 2 by nearly the same magnitude. Both curves are found to level off at large Ste_1, likely due to thermal conduction within the materials becoming the rate-limiting step when a sufficiently large external thermal stimulus is being provided. In contrast, Ste_2 influences the melting time very differently, as shown in Fig. 11(b). As expected, the melting time for layer 2 reduces sharply with increasing Ste_2, which is expected since Ste_2 represents how favorable the thermophysical properties of layer 2 are for melting. For example, increasing Ste_2 may imply reduced latent heat of melting for layer 2, which will clearly reduce the melting time for layer 2. In contrast, with Ste_1 held constant, increasing Ste_2 is found to not influence the melting time for layer 1. This is also expected since in Case I, the two layers melt in series, and, therefore, layer 1, which melts first, is completely unaffected by Stefan number for layer 2. This may also be seen mathematically through the lack of appearance of Ste_2 in Eqs. (1)-(6) that govern the melting of layer 1 in Case I.

In order to further illustrate the impact of Stefan number for Case I, Figs. 12(a) and 12(b) present melting front propagation plots for three different values of Ste_1 and Ste_2, respectively. Fig. 12(a) shows that as Ste_1 increases, the phase change propagation plot becomes steeper,

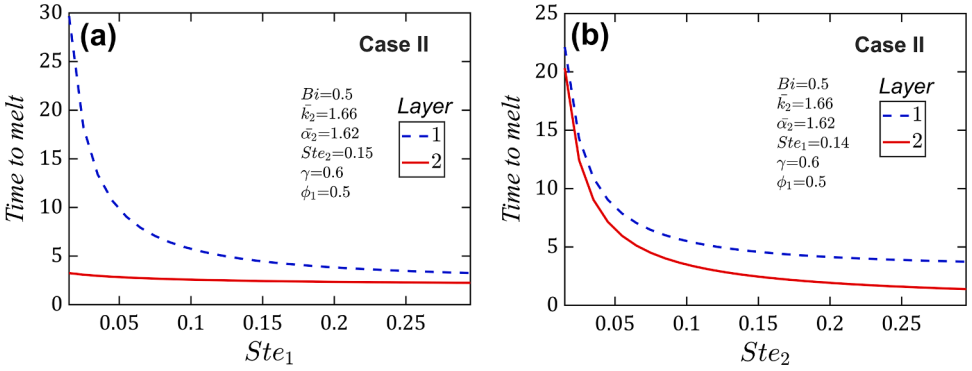

Fig. 13. Effect of Stefan numbers: Total melting time for each layer in Case II as functions of (a) Ste_1 (with $Ste_2 = 0.15$); (b) Ste_2 (with $Ste_1 = 0.14$). Values for other parameters are: $Bi = 0.5$, $\bar{k}_2 = 1.66$, $\bar{\alpha}_1 = 1.62$, $\phi_1 = 0.5$, $\gamma = 0.6$.

resulting in faster completion of the melting process in layer 1, with a similar impact on melting curves for layer 2 as well. In contrast, Fig. 12 (b) shows no impact of Ste_2 on the melting of layer 1 at all and a strong impact on melting of layer 2, both of which are consistent with Fig. 11 (b). It may be noted that increasing Ste_1 slightly increases the Stage B duration, which is the time needed time for the interfacial temperature to reach the melting temperature of layer 2, while changing Ste_2 does not affect the Stage B duration.

Similar plots for Case II, in which the lower-melting PCM is located away from the hot source are presented in Fig. 13 for $\gamma = 0.6$. Other problem parameter values are the same as Fig. 8. In Case II, both layers begin to melt in parallel. Therefore, it is expected that melting time for both layers will be sensitive to both Stefan numbers due to the parallel nature of the melting processes in the two layers. This is confirmed in Figs. 13(a) and 13(b), which present the melting time for both layers are functions of Ste_1 and Ste_2, respectively. As expected, Ste_1 influences melting in layer 1 more than in layer 2, whereas Ste_2 has a similar influence on both the layers. This is because for the chosen thicknesses, layer 1 completely melts only after layer 2 has finished melting. Once layer 2 melts, the heat supplied is used to melt layer 1 only. Therefore, speeding up the melting of layer 2 also speeds up the melting of layer 1 indirectly. In both cases, a saturation effect is observed, as expected, in that increasing the Stefan number has a reduced influence on melting time when the Stefan number is already quite large. This is due to thermal conduction in the materials starting to dominate over the phase change process in determining the rate of melting.

While several simplifying assumptions have been made in the theoretical model, such as neglecting natural convection and temperature-dependent properties, the analytical solution derived here helps understand the fundamental nature of the two-PCM melting problem, including the role of key non-dimensional parameters in this process. Note that the present work can be easily extended to cylindrical or spherical problems, with appropriate changes in the eigenfunctions that appear in several series solutions. Moreover, while presented as a melting problem, the solution derived here is equally applicable to the reverse problem of solidification of a two-PCM composite wall in contact with a cold body. Finally, the technique presented can also, in principle, be extended to more than two PCMs arranged in series. However, the number of possible arrangements of the PCMs in terms of their melting temperatures, and, therefore, the complexity of analysis increases rapidly with the number of PCMs. For example, the number of ways in which 3 or 4 PCMs can be arranged on the basis of their melting temperatures is 6 or 24, respectively, compared to only two cases needed to be considered for the two-PCM problem considered here.

6. Conclusions

While theoretical analysis of melting of a single PCM is quite common, including complications such as non-isothermal heat source, temperature-dependent properties and multi-dimensional phase change, the key contribution of the present work is the development of a theoretical model to predict temperature distribution and phase change propagation in a stack of two dis-similar PCMs arranged in series. The presence of two different materials leads to considerable complications such as two independent Stefan numbers, and series or parallel melting in both layers depending on melting temperatures relative to each other. This problem is systematically analyzed by considering two separate Cases, and multiple stages during each Case over time, some of which only involve sensible heating of the two layers. Amongst the key outcomes of the work presented here includes the identification of conditions in which the thermodynamically favorable simultaneous completion of melting in both layers may be accomplished. While the accuracy of the underlying eigenfunction series expansion method may reduce at large Stefan numbers, nevertheless, the key results derived here may be of benefit for a number of practical processes that are carried out in sufficiently mild operating conditions.

CRediT authorship contribution statement

Emad Hasrati: Formal analysis, Validation, Investigation, Data curation, Writing – original draft, Writing – review & editing. **Girish Krishnan:** Formal analysis, Validation, Investigation, Data curation, Writing – original draft, Writing – review & editing. **Ankur Jain:** Conceptualization, Methodology, Formal analysis, Validation, Investigation, Data curation, Project administration, Writing – original draft, Writing – review & editing.

Declaration of competing interest

The authors declare that they have no known competing financial interests or personal relationships that could have appeared to influence the work reported in this paper.

Data availability

Data will be made available on request.

References

[1] V.J. Lunardini, Heat Transfer with Freezing and Thawing, Elsevier, 1991.
[2] V. Alexiades, Mathematical Modeling of Melting and Freezing Processes, Routledge, 2018.
[3] A. Cohen, Encyclopedia of Thermal Packaging, Set 1: Thermal Packaging Techniques, World Scientific Press, 2012.
[4] I. Dincer, M.A. Rosen, Thermal Energy storage: Systems and Applications, John Wiley & Sons, 2021.
[5] R. Viskanta, Heat transfer during melting and solidification of metals, ASME J. Heat Transf. 110 (1988) 1205–1219, https://doi.org/10.1115/1.3250621.
[6] V.R. Voller, M. Cross, Estimating the solidification/melting times of cylindrically symmetric regions, Int. J. Heat Mass Transf. 24 (9) (1981) 1457–1462, https://doi.org/10.1016/0017-9310(81)90213-1.
[7] A. Mostafavi, M. Parhizi, A. Jain, Theoretical modeling and optimization of fin-based enhancement of heat transfer into a phase change material, Int. J. Heat Mass Transf. 145 (2019) 118698, https://doi.org/10.1016/j.ijheatmasstransfer.2019.118698, 1-10.
[8] D.A. Tarzia, A Bibliography on Moving-free Boundary Problems for the Heat Diffusion Equation. The Stefan and Related Problems, Firenze: Instituto Matematico, Ulisse Dini, 1988.
[9] G. Krishnan, M. Parhizi, A. Jain, Eigenfunction-based solution for solid-liquid phase change heat transfer problems with time-dependent boundary conditions, Int. J. Heat Mass Transf. 189 (2022) 122693, https://doi.org/10.1016/j.ijheatmasstransfer.2022.122693.
[10] M. Parhizi, A. Jain, Theoretical modeling of solid-liquid phase change in a phase change material protected by a multilayer Cartesian wall,', Int. J. Heat Mass Transf. 197 (2022) 123330 https://doi.org/10.1016/j.ijheatmasstransfer.2022.123330, 1-16.
[11] A. Jain, M. Parhizi, Theoretical analysis of phase change heat transfer and energy storage in a spherical phase change material with encapsulation,', Int. J. Heat Mass Transf. 185 (2022) 122348 https://doi.org/10.1016/j.ijheatmasstransfer.2021.122348, 1-12.
[12] T.R. Goodman, J.J. Shea, The Melting of Finite Slabs, J. Appl. Mech. 27 (1960) 16–24, https://doi.org/10.1115/1.3643893.
[13] M. Parhizi, A. Jain, Solution of the phase change Stefan problem with time-dependent heat flux using perturbation method, ASME J. Heat Transf. 141 (2) (2019), https://doi.org/10.1115/1.4041956.
[14] D.W. Hahn, M.N. Özisik, Heat Conduction, John Wiley & Sons, 2012.
[15] J. Lim, A. Bejan, J. Kim, Thermodynamic optimization of phase-change energy storage using two or more materials, J. Energy Resour. Technol. 114 (1992) 84–90, https://doi.org/10.1115/1.2905925.
[16] T. Kousksou, F. Strub, J. Lasvignottes, A. Jamil, J. Bédécarrats, Second law analysis of latent thermal storage for solar system, Solar Energy Mater. Solar Cells 91 (2007) 1275–1281, https://doi.org/10.1016/j.solmat.2007.04.029.
[17] R. Domański, G. Fellah, Exergy analysis for the evaluation of a thermal storage system employing PCMs with different melting temperatures, Appl. Therm. Eng. 16 (1996) 907–919, https://doi.org/10.1016/1359-4311(96)00003-8.
[18] T. Watanabe, A. Kanzawa, Second Law optimization of a latent heat storage system with PCMs having different melting points, Heat Recov. Syst. CHP 15 (1995) 641–653, https://doi.org/10.1016/0890-4332(95)90044-6.
[19] H. Michels, R. Pitz-Paal, Cascaded latent heat storage for parabolic trough solar power plants, Solar Energy 81 (2007) 829–837, https://doi.org/10.1016/j.solener.2006.09.008.
[20] S. Shaikh, K. Lafdi, C/C composite, carbon nanotube and paraffin wax hybrid systems for the thermal control of pulsed power in electronics, Carbon N Y 48 (2010) 813–824, https://doi.org/10.1016/j.carbon.2009.10.034.

[21] M. Ezra, Y. Kozak, V. Dubovsky, G. Ziskind, Analysis and optimization of melting temperature span for a multiple-PCM latent heat thermal energy storage unit, Appl. Thermal Eng. 93 (2016) 315–329, https://doi.org/10.1016/j.applthermaleng.2015.09.040.
[22] J. Wang, Y. Ouyang, G. Chen, Experimental study on charging processes of a cylindrical heat storage capsule employing multiple-phase-change materials, Int. J. Energy Res. 25 (2001) 439–447, https://doi.org/10.1002/er.695.
[23] T. Watanabe, H. Kikuchi, A. Kanzawa, Enhancement of charging and discharging rates in a latent heat storage system by use of PCM with different melting temperatures, Heat Recov. Syst. CHP 13 (1993) 57–66, https://doi.org/10.1016/0890-4332(93)90025-Q.
[24] W. Li, J. Wang, X. Zhang, X. Liu, H. Dong, Experimental and numerical investigation of the melting process and heat transfer characteristics of multiple phase change materials, Int. J. Energy Res. 44 (2020) 11219–11232, https://doi.org/10.1002/er.5718.
[25] T. Aldoss, M. Rahman, Comparison between the single-PCM and multi-PCM thermal energy storage design, Energy Conv. Manag. 83 (2014) 79–87, https://doi.org/10.1016/j.enconman.2014.03.047.
[26] Z.-X. Gong, A.S. Mujumdar, Enhancement of energy charge-discharge rates in composite slabs of different phase change, Int. J. Heat Mass Transf. 39 (1996) 725–733, https://doi.org/10.1016/0017-9310(95)00179-4.
[27] M. Fang, G. Chen, Effects of different multiple PCMs on the performance of a latent thermal energy storage system, Appl. Thermal Eng. 27 (2007) 994–1000, https://doi.org/10.1016/j.applthermaleng.2006.08.001.
[28] O. Elsanusi, E. Nsofor, Melting of multiple PCMs with different arrangements inside a heat exchanger for energy storage, Appl. Thermal Eng. 185 (2021) 116046, https://doi.org/10.1016/j.applthermaleng.2020.116046, 1-10.
[29] Ç. Susantez, Numerical investigation of latent heat thermal energy storage unit with different configurations and phase change materials, J. Energy Storage 54 (2022) 105279, https://doi.org/10.1016/j.est.2022.105279, 1-10.
[30] J. Wang, G. Chen, F. Zheng, Study on phase change temperature distributions of composite PCMs in thermal energy storage systems, Int. J. Energy Res. 23 (1999) 277–285, https://doi.org/10.1002/(SICI)1099-114X(19990325)23:4<277::AID-ER475>3.0.CO;2-Q.
[31] S. Shaikh, K. Lafdi, Effect of multiple phase change materials (PCMs) slab configurations on thermal energy storage, Energy Conv. Manag. 47 (2006) 2103–2117, https://doi.org/10.1016/j.enconman.2005.12.012.
[32] M.M. Farid, A. Kanzawa, Thermal performance of a heat storage module using PCM's with different melting temperatures: mathematical modeling, J. Sol. Energy Eng. 111 (1989) 152–157, https://doi.org/10.1115/1.3268301.
[33] C. Tittle, Boundary value problems in composite media: quasi-orthogonal functions, J. Appl. Phys. 36 (1965) 1486–1488, https://doi.org/10.1063/1.1714335.
[34] M.D. Mikhailov, M.N. Özisik, Unified Analysis and Solutions of Heat and Mass Diffusion, Dover Publications, 1994.
[35] D.V. Hale, M.J. Hoover, M.J. ONeill, Phase Change Materials Handbook, 1971,. No. NASA-CR-61363.
[36] S. Himran, A. Suwono, G.A. Mansoori, Characterization of alkanes and paraffin waxes for application as phase change energy storage medium, Energy Sources 16 (1994) 117–128, https://doi.org/10.1080/00908319408909065.